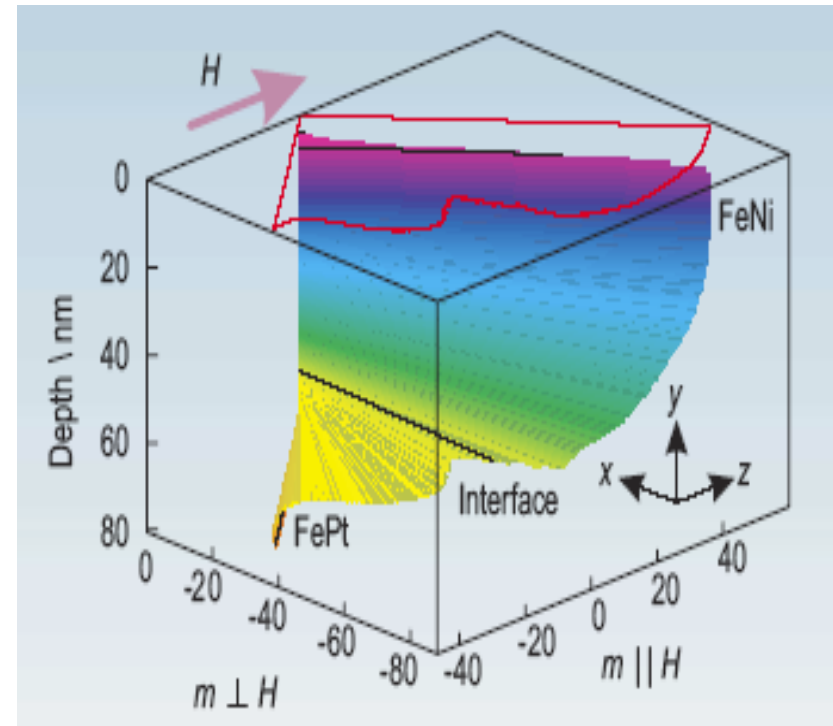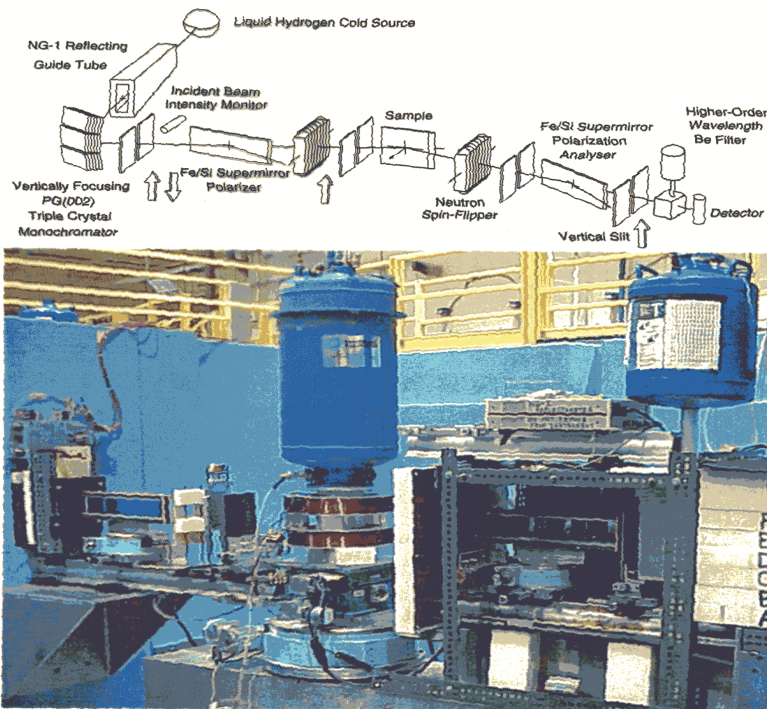# National School on Neutron and X-Ray Scattering

*Argonne and Oak Ridge National Laboratories*

Polarized Neutrons

*21 August 2012*



C.F.Majkrzak, *NIST Center for Neutron Research*,
Gaithersburg, MD

# Part 1: Neutron Polarization

<> a magnetic moment arises from the motion of electrical charges -- though neutral, a neutron is composed of charged quarks which give rise to a net magnetic dipole moment which is quantized with corresponding spin 1/2 -- a neutron is a Fermion

<> if it exists at all, any neutron electric dipole moment is of negligible magnitude for all practical purposes of concern to us here

<> a neutron can be represented by a spinor wave function having two components corresponding to two spin eigen-states (spin "+" or "up" and "-" or "down")

<> for a nucleus with spin, the neutron-nucleus (i.e., the *nuclear*) interaction is spin-dependent

<> the *magnetic* interaction between the neutron magnetic moment and that of a *nuclear* magnetic moment is relatively weak (and nuclear magnetic moments are normally not ordered -- a notable exception occurring in a 3He gas cell used as a neutron polarizer)

<> the *magnetic* interaction between the neutron magnetic moment and that of an atomic magnetic moment, on the other hand, can be comparable to the nuclear interaction

(a good description of the phenomenon of a quantized spin one-half system is given in the quantum mechanics text by Merzbacher)
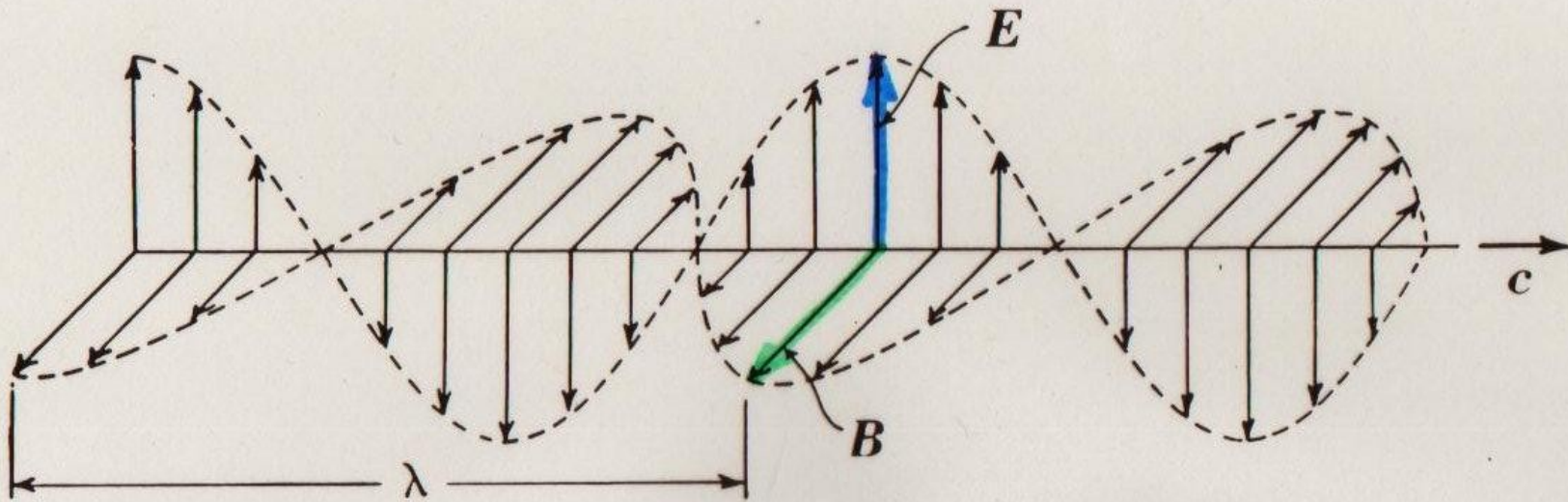
**Figure 41-15.** Representations of the electric and magnetic fields of a sinusoidal electromagnetic wave: (a) the field lines; (b) the sinusoidally varying amplitudes. (after Weidner & Sells, Elementary Classical Physics)
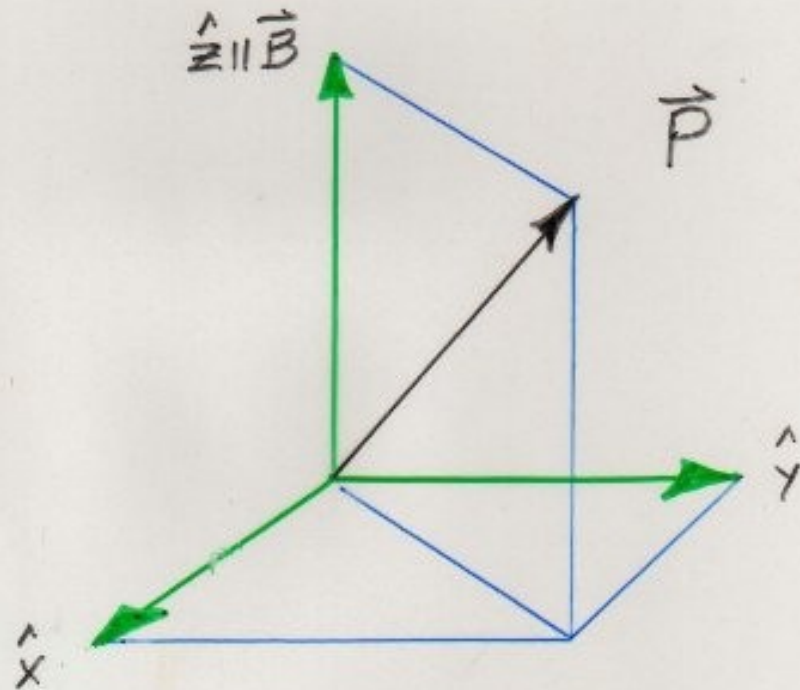
PHOTON

- ZERO MASS

- VELOCITY (IN VACUUM)

$$C_0 \cong 3 \times 10^8 \, m/sec$$

- POLARIZED ELECTROMAGNETIC WAVE

# NEUTRON WAVE FUNCTION

$$\Psi = C_+ \begin{pmatrix} 1 \\ 0 \end{pmatrix} e^{i\vec{k}_+ \cdot \vec{r}} + C_- \begin{pmatrix} 0 \\ 1 \end{pmatrix} e^{i\vec{k}_- \cdot \vec{r}}$$

$$k_\pm = n_\pm k_0$$

$$n_\pm^2 = 1 - \frac{2m}{(\hbar k_0)^2}(V_N \pm \mu B)$$

$$\psi = \psi_+ \begin{pmatrix} 1 \\ 0 \end{pmatrix} + \psi_- \begin{pmatrix} 0 \\ 1 \end{pmatrix} = \begin{pmatrix} \psi_+ \\ \psi_- \end{pmatrix}$$

$$= \underbrace{C_{0+} e^{ik_+ r}}_{C_+} \begin{pmatrix} 1 \\ 0 \end{pmatrix} + \underbrace{C_{0-} e^{ik_- r}}_{C_-} \begin{pmatrix} 0 \\ 1 \end{pmatrix}$$

$$= \underset{C_+}{\underbrace{\phantom{C_{0+} e^{ik_+ r}}}} + \underset{C_-}{\underbrace{\phantom{C_{0-} e^{ik_- r}}}}$$

where $C_{0+}$ and $C_{0-}$ are the values of $C_+$ and $C_-$
at $r = 0$, respectively,

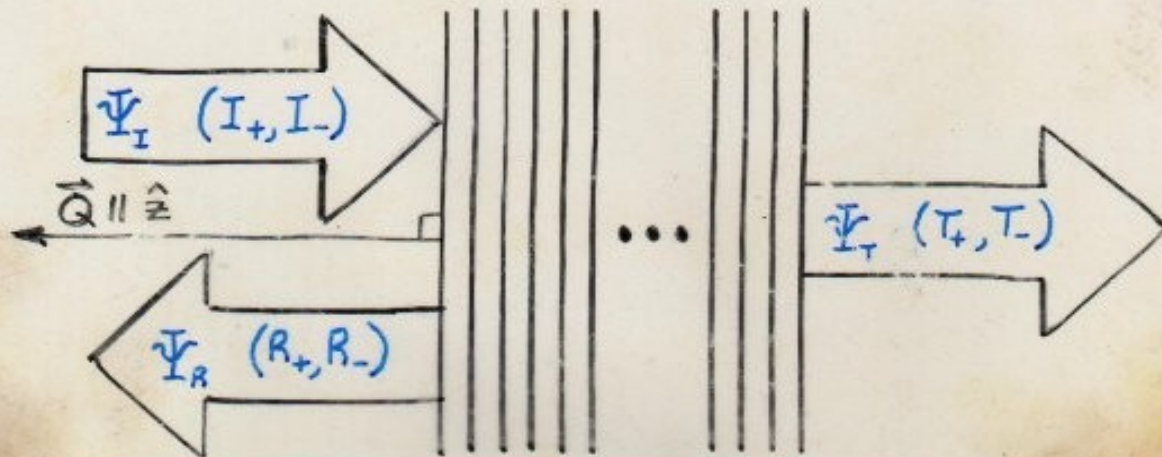$$k_\pm = M_\pm k_0 = k_0 \sqrt{1 - \frac{4\pi(\rho_N \pm \rho_M)}{k_0^2}}$$

and

$$\rho_N = N b \qquad \text{(nuclear scattering length density)}$$

$$\rho_M = \frac{m}{2\pi \hbar^2} \mu B \qquad \text{(magnetic scattering length density)}$$

# GENERAL MULTILAYER REFLECTIVITY
## CALCULATION FOR POLARIZED NEUTRONS

$$\left[\frac{-\hbar^2}{2m}\nabla^2 + (V-E)\right]\Psi = 0 \qquad \Psi = \begin{pmatrix} \psi_+ \\ \psi_- \end{pmatrix}$$



$\Psi_I \ (I_+, I_-)$

$\vec{Q} \parallel \hat{z}$

$\Psi_R \ (R_+, R_-)$

$\Psi_T \ (T_+, T_-)$

$$V_N = Nb$$
$$V_M = -\vec{\mu} \cdot \vec{B}$$

$$\frac{\partial^2}{\partial z^2}\psi_+ + \left(\frac{Q^2}{4} - 4\pi \rho_{11}\right)\psi_+ - 4\pi \rho_{12}\psi_- = 0$$

$$\frac{\partial^2}{\partial z^2}\psi_- + \left(\frac{Q^2}{4} - 4\pi \rho_{22}\right)\psi_- - 4\pi \rho_{21}\psi_+ = 0$$

$$\rho_{11} = Nb + Np \sin\theta \sin\phi$$
$$_{(22)} \qquad _{(-)}$$

$$\rho_{12} = Np\left(\cos\theta - i \sin\theta \cos\phi\right)$$
$$_{(21)} \qquad _{(+)}$$

$$\underline{V_M} = -\underline{\mu} \cdot \vec{B}$$

$$= -\gamma_m \left\{ \underline{S_x} B_x + \underline{S_y} B_y + \underline{S_z} B_z \right\}$$

$$= -\gamma_m \frac{\hbar}{2} \left\{ \begin{pmatrix} 0 & B_x \\ B_x & 0 \end{pmatrix} + \begin{pmatrix} 0 & -iB_y \\ iB_y & 0 \end{pmatrix} + \begin{pmatrix} B_z & 0 \\ 0 & -B_z \end{pmatrix} \right\}$$

$$= -\gamma_m \frac{\hbar}{2} \begin{pmatrix} B_z & B_x - iB_y \\ B_x + iB_y & -B_z \end{pmatrix}$$

$$= \frac{h^2}{2m\pi} \begin{pmatrix} N_{P_z} & N_{P_x} - iN_{P_y} \\ N_{P_x} + iN_{P_y} & -N_{P_z} \end{pmatrix}$$

- ONLY COMPONENTS OF $\vec{B} \perp \vec{Q}$ ARE EFFECTIVE IN SCATTERING NEUTRONS

$$\underline{\mu} = -\gamma_m \frac{\hbar}{2} \left\{ \begin{pmatrix} 0 & 1 \\ 1 & 0 \end{pmatrix} \hat{x} + \begin{pmatrix} 0 & -i \\ i & 0 \end{pmatrix} \hat{y} + \begin{pmatrix} 1 & 0 \\ 0 & -1 \end{pmatrix} \hat{z} \right\}$$

## PIECEWISE CONTINUOUS SOLUTION :

$$\begin{pmatrix} T_+ \\ T_- \\ i\frac{Q}{2}T_+ \\ i\frac{Q}{2}T_- \end{pmatrix} = \widehat{M}_\Pi \begin{pmatrix} I_+ + R_+ \\ I_- + R_- \\ i\frac{Q}{2}[I_+ - R_+] \\ i\frac{Q}{2}[I_- - R_-] \end{pmatrix}$$

WHERE $|T_+|^2, |T_-|^2$ ARE THE TRANSMISSION PROBABILITIES

AND $|R_+|^2, |R_-|^2$ ARE THE REFLECTION PROBABILITIES

$$\widehat{M}_\Pi = \prod_{\ell=L}^{1} \widehat{M}_\ell$$

( $\widehat{M}_\ell$ IS A 4X4 "TRANSFER" MATRIX CORRESPONDING TO THE $\ell$ TH LAYER OF A MULTILAYER STRUCTURE )
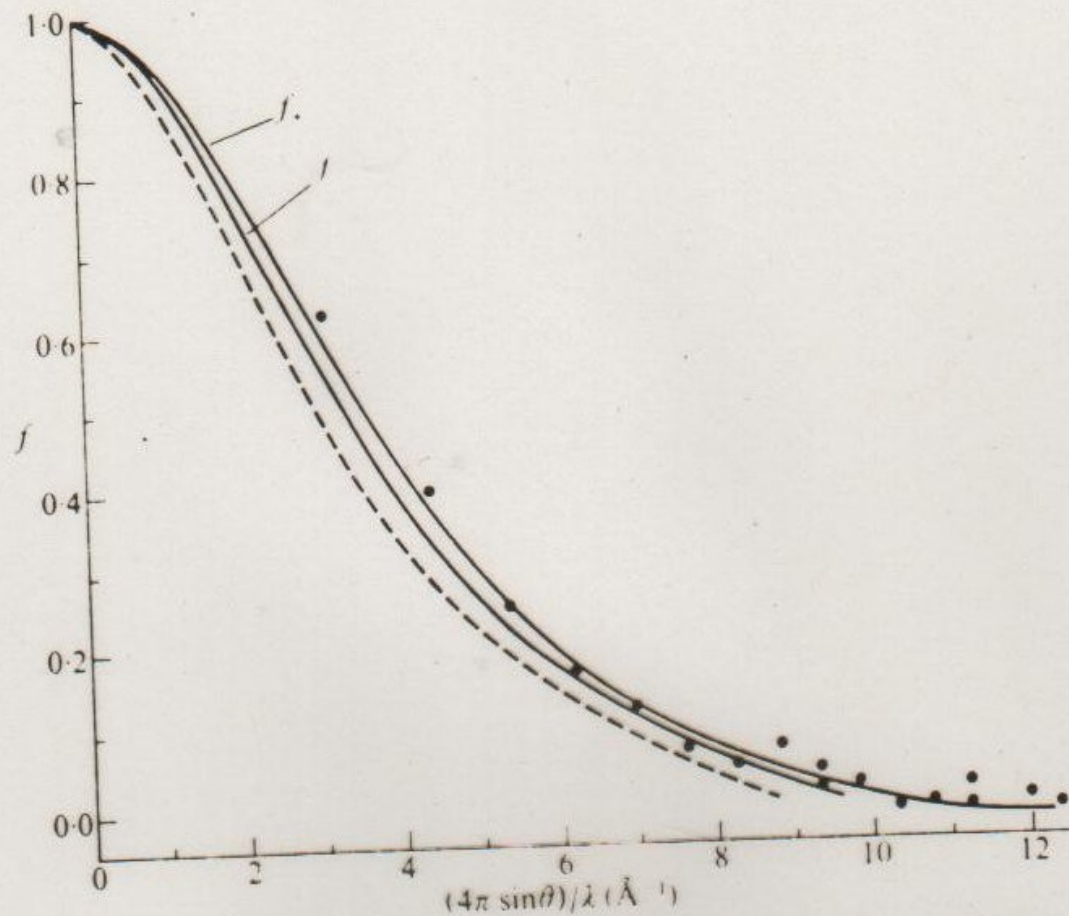
FIG. 126. Magnetic form factor curves for iron. The full-line curves show the calculation by Wood and Pratt for, respectively, the five 3d electrons of +ve spin and the single 3d electron of −ve spin for a free iron atom. The points are the experimental measurements of Shull and Yamada for metallic iron. The broken-line curve contrasts the experimental data for the $Fe^{3+}$ ion in magnetite.
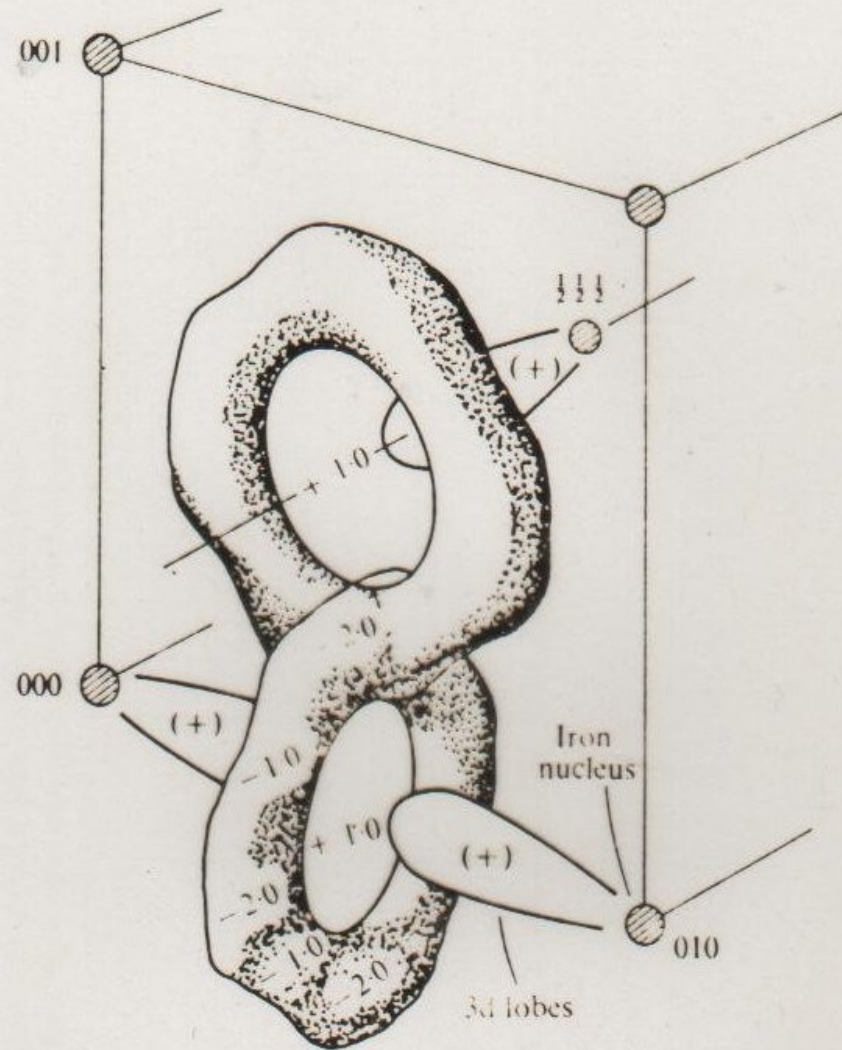
FIG. 134. The residual magnetization (kG) in iron as deduced experimentally by Shull and Mook (1966). The positive excess of 3d magnetization along the cube edges is over-emphasized in comparison with the interlocking rings of negative magnetization. The rings shown are centred on $0\frac{1}{2}0$, $0\frac{1}{2}\frac{1}{2}$.

— x-rays DO interact with magnetic as well as with electronic charge distributions

— for x-rays, $\dfrac{I_{MAGN.}}{I_{CHARGE}} \sim 10^{-6}$

→ magn. scatt. of x-rays is a relativistic effect )

( non-resonant )

— $r_{CHARGE} \propto FT(\text{charge density}) \cdot C$

$r_{MAGN.} \propto \frac{1}{2} FT(\overset{(L)}{\text{orbital density}}) \cdot A$

$+ FT(\overset{(S)}{\text{spin density}}) \cdot B$

when A, B, & C give the pol. dep. of the scattering

— for neutrons, $\mu \propto \mu_B (L + 2S)$ so that L & S contr. can't be <u>directly</u> separated ( because spatial extents of magn. dens. of L & S contrib. are diff., modelling & fitting allows for separation )

Non-resonant magnetic x-ray scattering in UAs (0,½,4)
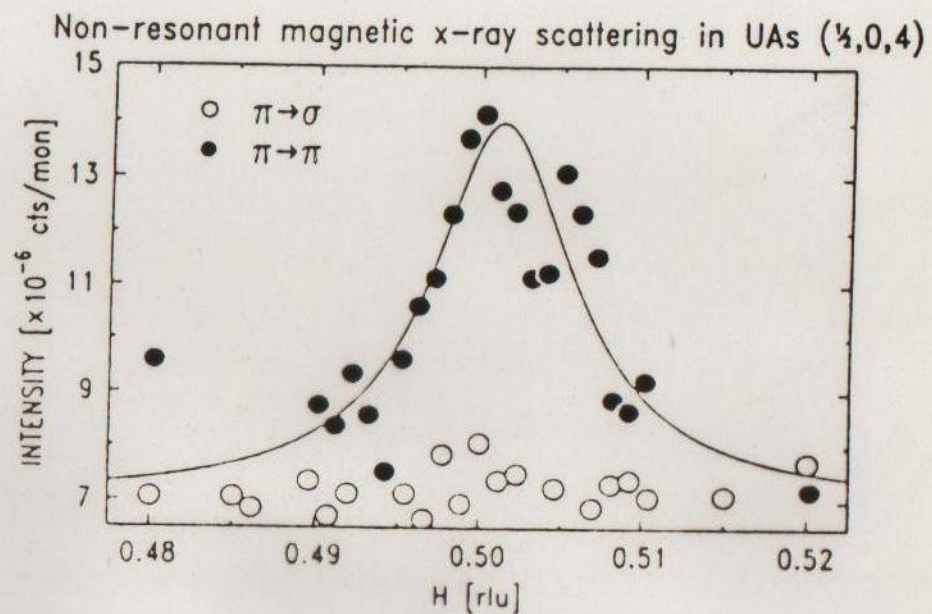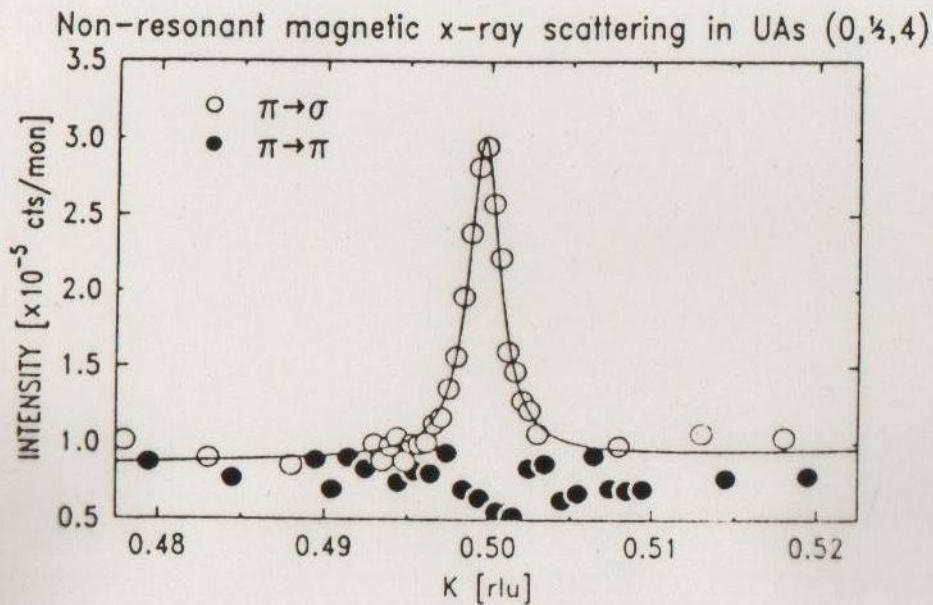
Non-resonant magnetic x-ray scattering in UAs (½,0,4)

Fig. 2: Experimental results taken with different polarization (as indicated) for the satellites around the (004) charge peak in UAs. Based on Eq. (4) and our understanding of the magnetic structure (from neutrons) the structure factors are proportional to:

left hand side:  $(\pi \to \pi)$  zero         $(\pi \to \sigma)$  (L + S)
right hand side:  $(\pi \to \pi)$  (~ 0.5L + S)   $(\pi \to \sigma)$  (~ 0.1 S)

(AFTER G. LANDER et al.)

— resonant magnetic x-ray scatt.:
e.g. in Ho at an x-ray energy near
the L(III) absorption edge, the inc.
photon excites a 3p electron to
the 5d unoccupied level — under these
conditions electric $2^L$ pole resonances
are stimulated and contribute to
the coherent scattering amplitude!
can roughly describe this process
as one in which a core electron
is excited to an unoccupied level
and forms a _magnetic resonance_
with the _unpaired electrons_ in
that particular shell

— resonant enhancement as large
   as $10^6$!
— resonant magn. scatt. is element
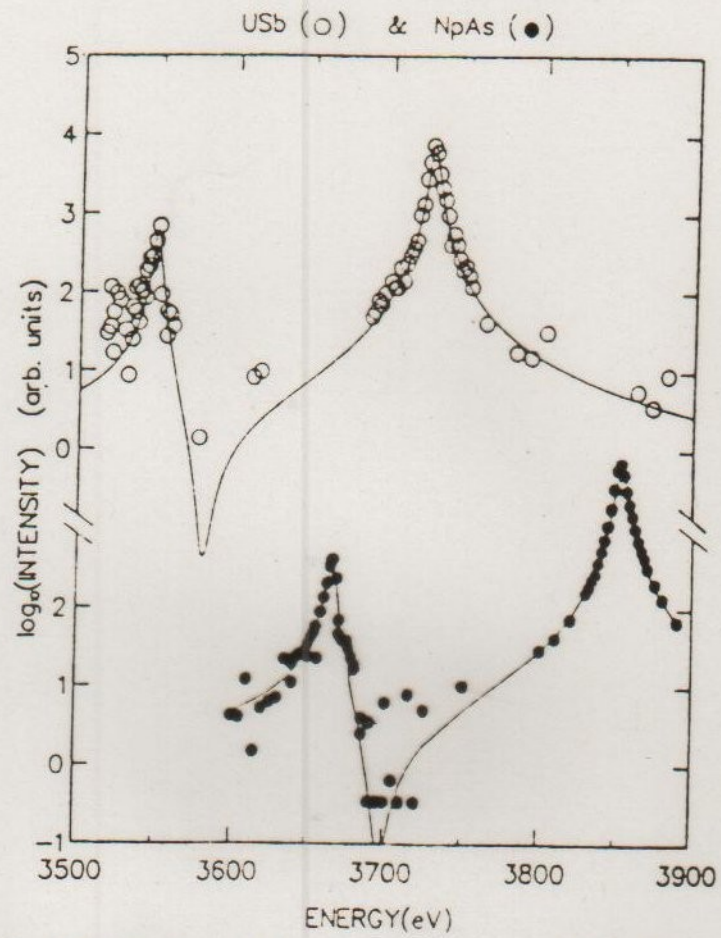specific

USb (O) & NpAs (●)



Fig. 3: Intensity of the magnetic satellite from a uranium and neptunium compound as a function of energy. The solid lines are fits to atomic resonance theory. (Taken from Ref. 24 and 25)

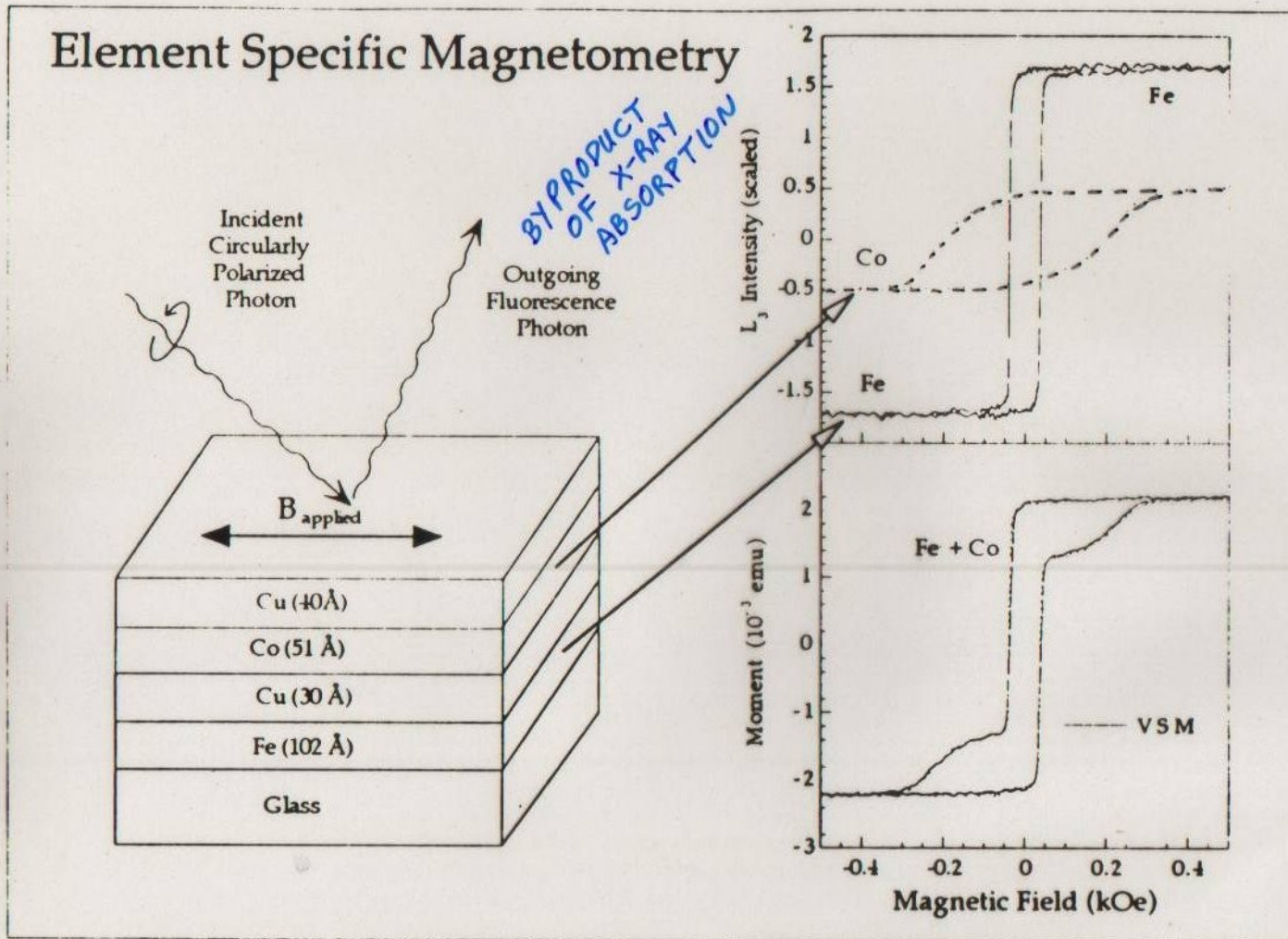(D. GIBBS et al.)    (G. LANDER et al.)

**Figure 3.** Element specific magnetometry. Multilayer structure (left) indicates the hysteresis loop (top right) associated with Fe (solid) and Co (dashed) measured from the resonant $L_3$ white-line intensity vs. applied field for comparison (bottom right) of summed Fe+Co (dashed) with total moment (solid) hysteresis loop.

SOFT X-RAY MAGNETIC CIRCULAR DICHROISM

(Y. IDZERDA et al.)

ABSORPTION OF CIRCULARLY POLARIZED PHOTONS AT MAGNETICALLY INTERESTING $2p \rightarrow 3d$ TRANSITIONS IS AN ELEMENT SPECIFIC PROBE OF MAGNETIC ORDER AND STRUCTURE

PHOTON "SPIN" (RT. OR LT. CIRCULAR POL.) ALIGNED OR ANTI-ALIGNED TO ELECTRON SPIN

# Reflection and Transmission of Polarized Neutrons Involving Magnetic Potentials

Given the existence of two different spin states of the neutron, a general magnetic interaction potential must be able to account for two qualitatively different types of possible scattering processes -- one which results in a change of the initial spin state, and another which does not. Consequently, the description of specular reflection from a flat magnetic film structure requires a *pair* of *coupled*, one-dimensional wave equations (the spin quantization axis is taken to be z whereas the direction of propagation of the wave is along the x-axis):

$$\left[ \frac{-\hbar^2}{2m} \frac{\partial^2}{\partial x^2} \begin{pmatrix} 1 & 0 \\ 0 & 1 \end{pmatrix} + \begin{pmatrix} V_{++} & V_{+-} \\ V_{-+} & V_{--} \end{pmatrix} - E \begin{pmatrix} 1 & 0 \\ 0 & 1 \end{pmatrix} \right] \begin{pmatrix} \psi_+ \\ \psi_- \end{pmatrix} = 0$$

The interaction potentials can be, in general, spin-dependent and derive from both nuclear and magnetic interactions between neutron and matter. As shown in detail in the quantum mechanics text by Merzbacher (Chapters 12 & 13, pages 251 to 293), the magnetic interaction must be represented by an operator appropriate for the quantum spinor nature of the neutron magnetic moment:

$$\breve{V}_M = \vec{\mu} \cdot \vec{B} = -\mu \vec{\sigma} \cdot \vec{B} = -\mu(\breve{\sigma}_x B_x + \breve{\sigma}_y B_y + \breve{\sigma}_z B_z)$$

$$= -\mu \left[ \begin{pmatrix} 0 & 1 \\ 1 & 0 \end{pmatrix} B_x + \begin{pmatrix} 0 & -i \\ i & 0 \end{pmatrix} B_y + \begin{pmatrix} 1 & 0 \\ 0 & -1 \end{pmatrix} B_z \right] = -\mu \begin{bmatrix} B_z & B_x - iB_y \\ B_x + iB_y & -B_z \end{bmatrix}$$

where $\mu$ is the magnitude of the magnetic moment of the neutron, $\breve{\sigma}$ is the Pauli spin operator, and $\vec{B}$ is the magnetic field. Previously, the scalar, non-spin-dependent nuclear potential was written as

$$V_N = \frac{2\pi\hbar^2}{m} Nb = \frac{2\pi\hbar^2}{m} \rho_N$$

The magnetic potential can also be expressed in terms of scattering length densities as

$$\breve{V}_M = \frac{2\pi\hbar^2}{m} \begin{pmatrix} \rho_{Mz} & \rho_{Mx} - i\rho_{My} \\ \rho_{Mx} + i\rho_{My} & -\rho_{Mz} \end{pmatrix}$$

Combining nuclear and magnetic potentials we obtain

$$V_N + \breve{V}_M = \frac{2\pi\hbar^2}{m} \begin{pmatrix} \rho_N + \rho_{Mz} & \rho_{Mx} - i\rho_{My} \\ \rho_{Mx} + i\rho_{My} & \rho_N - \rho_{Mz} \end{pmatrix} = \frac{2\pi\hbar^2}{m} \begin{pmatrix} \rho_{++} & \rho_{+-} \\ \rho_{-+} & \rho_{--} \end{pmatrix}$$

In terms of the scattering length densities, the coupled wave equations of motion are

$$\left[ \frac{\partial^2}{\partial x^2} + k_{0x}^2 - 4\pi\rho_{++} \right] \psi_+ - 4\pi\rho_{+-} \psi_- = 0$$

$$\left[ \frac{\partial^2}{\partial x^2} + k_{0x}^2 - 4\pi\rho_{--} \right] \psi_- - 4\pi\rho_{-+} \psi_+ = 0$$

In the special case where all magnetic fields are taken to be along the defined z-axis of quantization, $\rho_{+-} = \rho_{-+} = 0$ and the wave equations become decoupled, each describing one of the two pure spin eigenstates independently. The expressions for the reflection and transmission amplitudes associated with each of the two uncoupled equations then become essentially equivalent to those derived for the nonmagnetic case in Figure 3. For the time being, this is all we should need.

$$\Psi(x, S_{\pm}) = C_{0_+}\begin{pmatrix}1\\0\end{pmatrix}e^{im_{x_+}k_{0x}x} + C_{0_-}\begin{pmatrix}0\\1\end{pmatrix}e^{im_{x_-}k_{0x}x}$$

$$\underbrace{\phantom{C_{0_+}\begin{pmatrix}1\\0\end{pmatrix}e}}_{\chi_+} \qquad \underbrace{\phantom{C_{0_-}\begin{pmatrix}0\\1\end{pmatrix}}}_{\chi_-}$$

The magnetic field defining the quantization axis is taken to be parallel to $\hat{z}$.

$$m_{x_\pm} = \sqrt{1 - \frac{4\pi(\rho_N \pm \rho_M)}{k_{0x}^2}} \qquad \text{where } \rho_M = \frac{m}{2\pi\hbar^2}\mu B$$
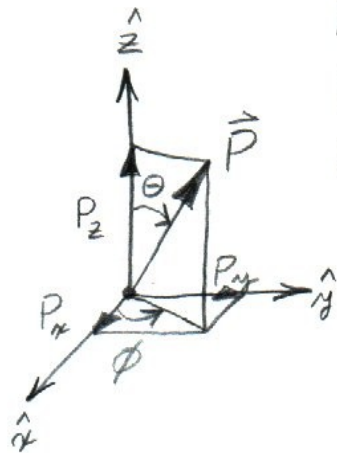
$$\chi^{*T}\chi = \begin{pmatrix}c_+^* & c_-^*\end{pmatrix}\begin{pmatrix}C_+\\C_-\end{pmatrix} = \underbrace{|C_+|^2}_{} + \underbrace{|C_-|^2}_{} = 1$$

probability of being + or −, respectively

$$\vec{P} = P_x\,\hat{x} + P_y\,\hat{y} + P_z\,\hat{z}$$

$$P_x = \sin\theta\cos\phi = 2\,\mathrm{Re}\,(C_+^* C_-)$$
$$P_y = \sin\theta\sin\phi = 2\,\mathrm{Im}\,(C_+^* C_-)$$
$$P_z = \cos\theta = |C_+|^2 - |C_-|^2$$



| $P_x$ | $P_y$ | $P_z$ | $\theta$ | $\phi$ | $C_+$ | $C_-$ |
|---|---|---|---|---|---|---|
| 0 | 0 | 1 | 0 | 0 | 1 | 0 |
| 0 | 0 | −1 | $\pi$ | 0 | 0 | 1 |
| 1 | 0 | 0 | $\pi/2$ | 0 | $1/\sqrt{2}$ | $1/\sqrt{2}$ |
| 0 | 1 | 0 | $\pi/2$ | $\pi/2$ | $1/\sqrt{2}$ | $i/\sqrt{2}$ |

$$|\Psi|^2 \equiv \Psi^{*T}\Psi = \left[\Psi_+\binom{1}{0}+\Psi_-\binom{0}{1}\right]^{*T}\left[\Psi_+\binom{1}{0}+\Psi_-\binom{0}{1}\right]$$

$$= \binom{\Psi_+}{\Psi_-}^{*T}\binom{\Psi_+}{\Psi_-} = \left(\Psi_+^*\ \ \Psi_-^*\right)\binom{\Psi_+}{\Psi_-}$$

$$= \Psi_+^*\Psi_+ + \Psi_-^*\Psi_- = C_{a_+}^*e^{-ik_+r}\,C_{a_+}e^{+ik_+r} + C_{0_-}^*e^{-ik_-r}\,C_{0_-}e^{+ik_-r}$$

$$= |C_{0_+}|^2 + |C_{0_-}|^2 = 1$$

$$P_x(r) = 2\,Re\left(C_{I_+}^*\,C_{I_-}\right)$$

$$= 2\,Re\left[C_{0_{I_+}}^*e^{-ik_+r}\ \ C_{a_{I_-}}e^{+ik_-r}\right]$$

$$= 2\,Re\left[\left(\tfrac{1}{\sqrt{2}}\right)\left(\tfrac{1}{\sqrt{2}}\right)e^{i(k_- - k_+)r}\right]$$

$$= (2)\left(\tfrac{1}{2}\right)Re\left[\cos(k_- - k_+)r\right]$$

$$P_x(r) = \cos\left[(m_- - m_+)k_0 r\right]$$

# APPENDIX PN: NEUTRON POLARIZATION FORMULAS
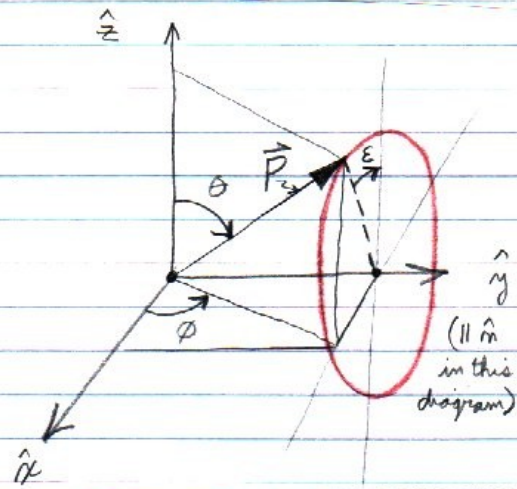


**Polarization Vector**

$$\vec{P} = P_x \hat{x} + P_y \hat{y} + P_z \hat{z}$$

$$P^2 = P_x^2 + P_y^2 + P_z^2 = 1$$

$$P_x = \sin\theta\cos\phi = 2\,Re(C_+^* C_-)$$

$$P_y = \sin\theta\sin\phi = 2\,Im(C_+^* C_-)$$

$$P_z = \cos\theta = |C_+|^2 - |C_-|^2$$

$C_\pm = $ spinor wave function coefficients

---

**Pauli Spin Operator**

$$\check{\sigma} = \begin{pmatrix} 0 & 1 \\ 1 & 0 \end{pmatrix}\hat{x} + \begin{pmatrix} 0 & -i \\ i & 0 \end{pmatrix}\hat{y} + \begin{pmatrix} 1 & 0 \\ 0 & -1 \end{pmatrix}\hat{z} = \check{\sigma}_x \hat{x} + \check{\sigma}_y \hat{y} + \check{\sigma}_z \hat{z}$$

$$\vec{P} = \langle \check{\sigma}_x \rangle \hat{x} + \langle \check{\sigma}_y \rangle \hat{y} + \langle \check{\sigma}_z \rangle \hat{z}$$

$$\check{I} = \begin{pmatrix} 1 & 0 \\ 0 & 1 \end{pmatrix}$$

---

**Rotation Operator**

$$\check{U}_R(\varepsilon, \hat{m}) = \check{I}\cos\left(\tfrac{\varepsilon}{2}\right) - i\,\hat{m}\cdot\check{\sigma}\,\sin\left(\tfrac{\varepsilon}{2}\right) = e^{-i\left(\tfrac{\varepsilon}{2}\right)\hat{m}\cdot\check{\sigma}}$$

$\varepsilon = $ angle of rotation $\qquad \hat{m} = $ axis of rotation

---

| | |
|---|---|
| $|C_+|^2 + |C_-|^2 = 1$ | $|C_+|^2 = \dfrac{N_+}{N_+ + N_-}$ |
| $P_z = \dfrac{N_+ - N_-}{N_+ + N_-}$ | $|C_-|^2 = \dfrac{N_-}{N_+ + N_-}$ |
| $C_+ = \cos\left(\tfrac{\theta}{2}\right)$ | $\Psi = \Psi_+ \begin{pmatrix}1\\0\end{pmatrix} + \Psi_- \begin{pmatrix}0\\1\end{pmatrix} = \begin{pmatrix}\Psi_+\\\Psi_-\end{pmatrix}$ |
| $C_- = \sin\left(\tfrac{\theta}{2}\right)e^{i\phi}$ | $= C_{o+}\,e^{ik_+ r}\begin{pmatrix}1\\0\end{pmatrix} + C_{o-}\,e^{ik_- r}\begin{pmatrix}0\\1\end{pmatrix}$ |
| | $|\Psi|^2 = (\Psi_+^* \;\; \Psi_-^*)\begin{pmatrix}\Psi_+\\\Psi_-\end{pmatrix} = |C_{o+}|^2 + |C_{o-}|^2 = 1$ |

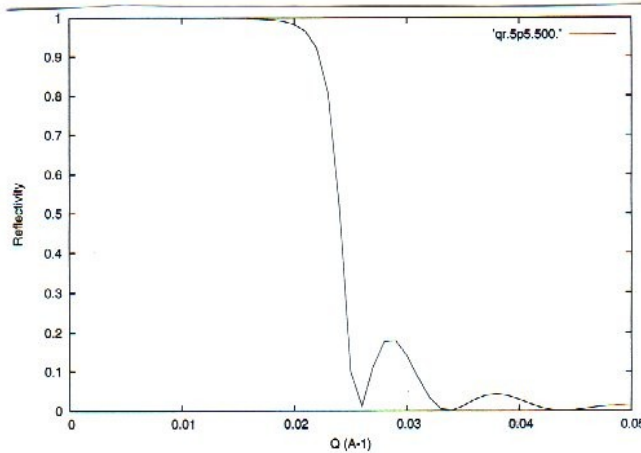# NEUTRON POLARIZER

By reflection from a magnetic film with nuclear and magnetic scattering length densities such that $P_N - P_M = 0$ (for "−" spin state) and $P_N + P_M \neq 0$ (for "+" spin state).

$\vec{k_I}$  $\boxed{P_{Iz} = 0}$  $\hat{z} \parallel \vec{B} \parallel \vec{M}$  $|r_+|^2 = 1$  $\boxed{P_{Rz} = +1}$

$\theta$  $\theta$  $\vec{k_F}$  $\hat{y}$

$\hat{x}$

$|t_-|^2 = 1$

$\boxed{P_{Tz} = -1}$

$|r_+|^2$
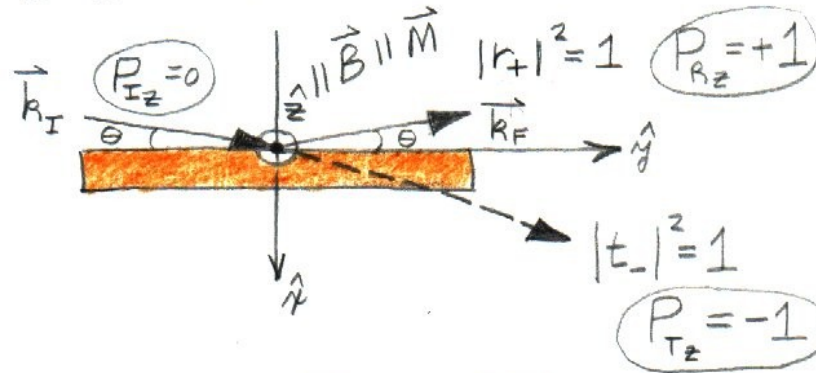
$(|r_-|^2 = 0,$

$|t_-|^2 = 1)$

(CALCULATED USING FORMULAS OF FIGURE 3)
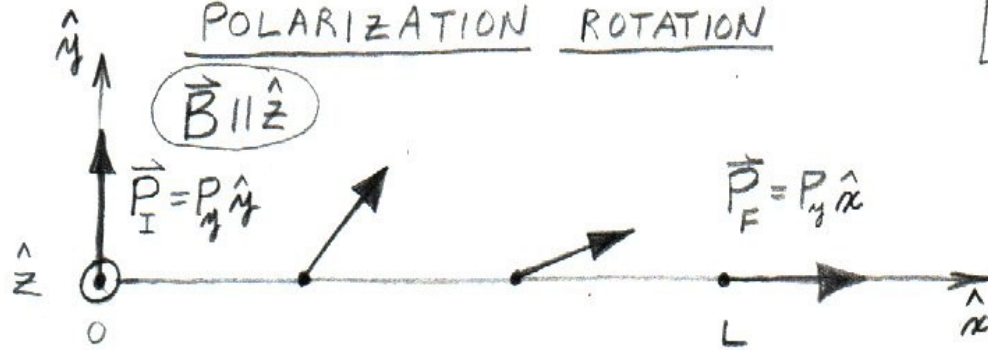
Reflectivity vs $Q (Å^{-1})$, curve labeled 'qr.5p5.500.'

$Q = 2 k_{0x} = 2 k_0 \sin \theta$

$P_N + P_M = 10.0 \times 10^{-6} \, Å^{-2}$

$P_N - P_M = 0.0$

$L = 500. \, Å$

$\boxed{\vec{B} \parallel \hat{z}}$

$\vec{P}_I = P_y \hat{y}$          $\vec{P}_F = P_y \hat{x}$

$$\psi = \underbrace{C_{o_+} e^{i m_{x_+} k_{ox} x} \binom{1}{0}}_{C_+} + \underbrace{C_{o_-} e^{i m_{x_-} k_{ox} x} \binom{0}{1}}_{C_-}$$

$$C_\pm(x) = C_{o_\pm}\left[\cos\left(m_{x_\pm} k_{ox} x\right) + i \sin\left(m_{x_\pm} k_{ox} x\right)\right]$$

$\frac{1}{\sqrt{2}}$

$$P_x(x) = 2\,\mathrm{Re}(C_+^* C_-) = \cos\left[(m_{x_-} - m_{x_+}) k_{ox} x\right]$$

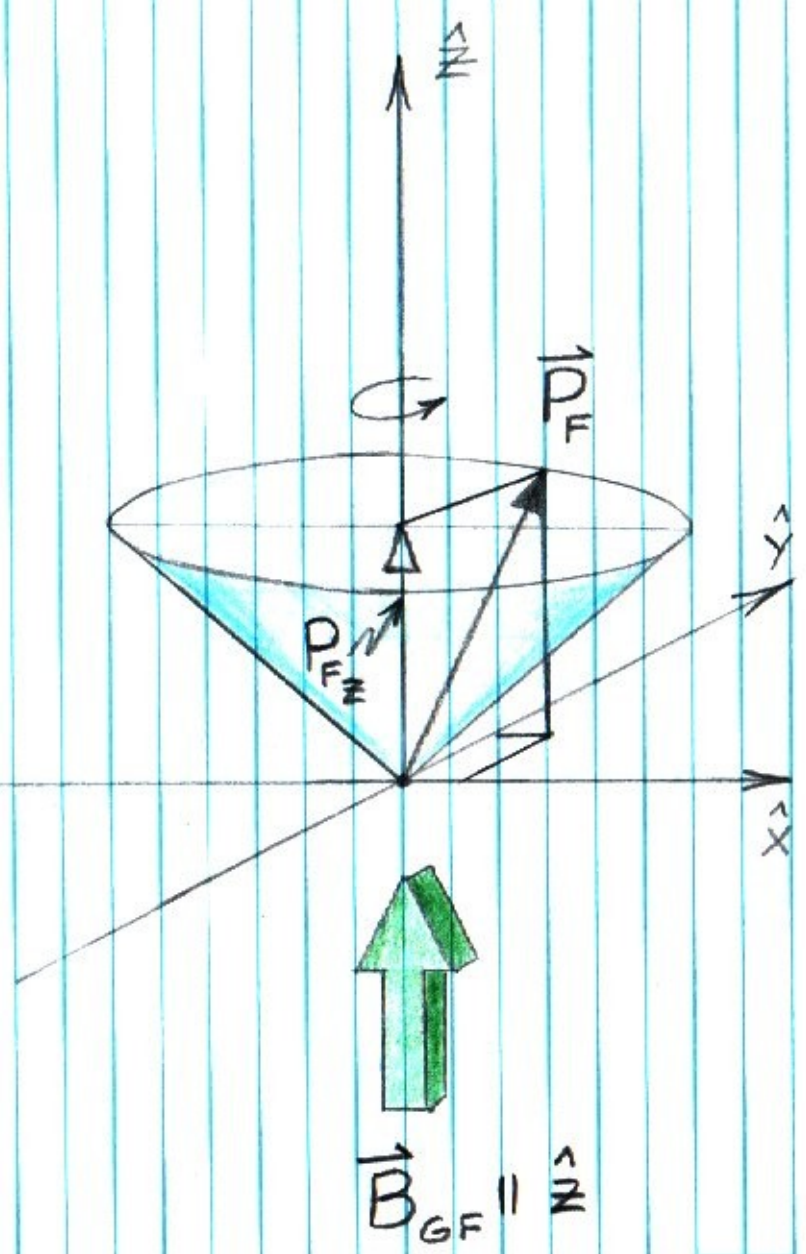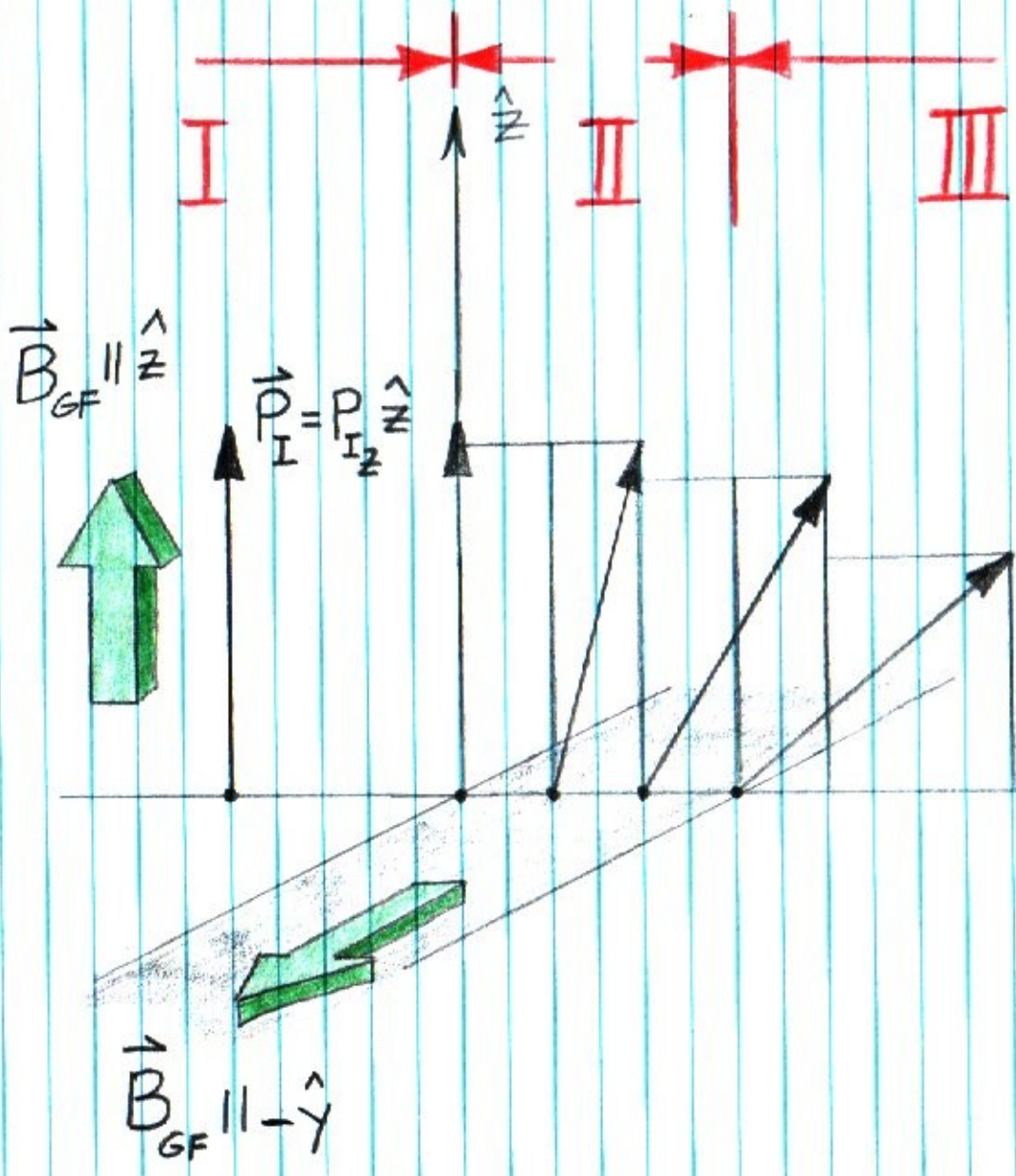$$P_y(x) = 2\,\mathrm{Im}(C_+^* C_-) = \sin\left[(m_{x_-} - m_{x_+}) k_{ox} x\right]$$

$$P_z(x) = |C_+|^2 - |C_-|^2 = 0$$

(Note that the z component of the polarization — along the quantization axis — remains unchanged at zero value through this rotation.)

$$(m_{x_-} - m_{x_+}) k_{ox} x =$$

$$\left[\sqrt{1 - \frac{2m\mu B}{(\hbar k_{ox})^2}} - \sqrt{1 + \frac{2m\mu B}{(\hbar k_{ox})^2}}\right] k_{ox} x$$

$$\simeq \frac{2m\mu B}{(\hbar k_{ox})^2} k_{ox} x$$

$\vec{B}_{GF} \parallel \hat{z}$

$\vec{P}_I = P_{I_z} \hat{z}$

$\hat{z}$

$\vec{B}_{GF} \parallel -\hat{y}$

$\vec{P}_F$

$P_{F_z}$

$\hat{z}$

$\hat{y}$

$\hat{x}$

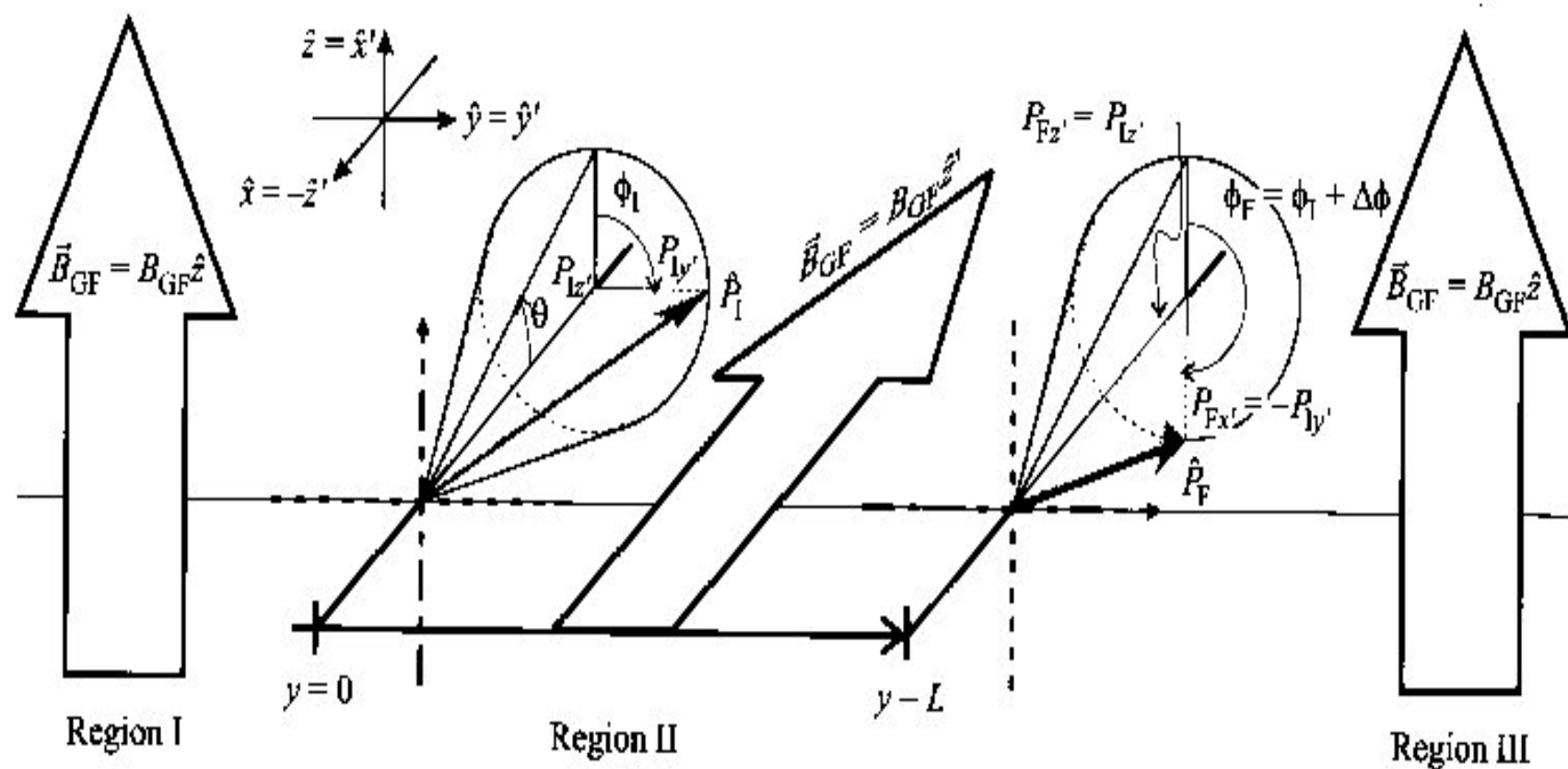$\vec{B}_{GF} \parallel \hat{z}$

I    II    III

Fig. 11. Magnetic guide field configuration along the neutron trajectory ($y$ axis) similar to that shown in Figure 10, but for a more general initial neutron polarization at $y = 0$. Note that as the neutron polarization precesses through Region II, its projection along the field direction ($z'$ axis) remains constant. The component along the $y'$ axis, however, is rotated to point along the $-x'$ axis at $y = L$.

# Part 2: Application of Polarized Neutrons in Scattering Studies of Magnetic Condensed Matter

<> elastic scattering to determine magnetic *structures*

<> inelastic scattering to probe magnetic *excitations* such as spin waves

G.E. BACON

# 6

# THE PRINCIPLES OF MAGNETIC SCATTERING

## 6.1. Introduction

AT the beginning of Chapter 2 we explained that, whereas in general the scattering of neutrons by atoms was a nuclear process, nevertheless an exception occurred with magnetic atoms, in the case of which there is additional scattering on account of an interaction between the neutron magnetic moment and the magnetic moment of the atom. We return in this chapter to a discussion of the principles of magnetic scattering and will proceed in the following two chapters to a detailed account of magnetic form-factors and of the way particular types of magnetic structure are revealed.

The determination of the magnetic structures of materials is a task which can achieved only by making measurements of the scattering of neutrons. Indeed it is true to say that our whole conception of the existence of a 'magnetic architecture' within the atomic structure of solids has arisen from observations with neutrons.

The elements of the first transition series which includes iron, cobalt, and nickel, have incomplete 3d shells, as indicated in Table 12 which lists the electronic structures of the free atoms with atomic numbers 19–30. The arrangements of the 3d and 4s shells of some free atoms and ions are shown in Table 13 which also gives the number of unpaired electrons and the spectroscopic ground terms of the ions. These unpaired electrons give rise to a resultant magnetic moment. Interaction of this with the magnetic moment of the neutron, which has a spin quantum number of $\frac{1}{2}$ and a magnetic moment of 1·9 nuclear magnetons, produces neutron scattering which is additional to that produced by the nucleus.

It is worth noting in passing that the fact the neutron, which is an uncharged particle, possesses a magnetic moment is anomalous. A likely explanation is that a neutron spends part of its time dissociated into a proton and a negative $\pi$-meson, and although the centres of their respective positive and negative charges do coincide yet the negative charge is more diffuse. This would cause the neutron

# POLARIZED NEUTRON REFLECTOMETRY

C.F.Majkrzak (National Institute of Standards and Technology)

Historically, neutron elastic scattering studies have provided a wealth of important atomic scale information about the magnetic structures of condensed matter, a significant part of which could not have been obtained by any other means. In the beginning, magnetic neutron diffraction research was performed primarily on bulk crystals. In more recent years, advances in thin film deposition techniques have made it possible to synthesize a variety of new types of layered magnetic systems, with properties that can be tailored for studies of fundamental scientific interest as well as technological applications. Throughout this still ongoing development, neutron scattering techniques, especially polarized neutron reflectometry (PNR) and diffraction, have made and continue to make significant contributions to the understanding of the physical behavior of magnetic thin films and superlattices (see, for example, the references [1,2]).

Polarized neutron reflectometry can be divided into two broad categories, one of which corresponds to reflection measurements performed with the wavevector transfer Q normal to the film surface, commonly referred to as specular reflectometry, and the other to scattering done with some component of Q lying in the plane of the film. Analysis of the specular polarized neutron reflectivity, measured as a function of Q, yields the in-plane average of the vector magnetization depth profile along the surface normal, with a spatial resolution of less than a nanometer in certain cases. The nonspecular reflectivity, on the other hand, reveals in-plane magnetic structure, such as that associated with domains or artificially patterned surfaces.

In this presentation, we will first show why PNR is such an extraordinarily sensitive, and in some regards unique, probe of magnetic order in thin films and multilayers. We will also illustrate how state-of-the-art methods in experimental and theoretical PNR (see, for example, [3]) can be applied to study current problems in magnetism, including investigations of magnetic semiconductor films and superlattices [4], of particular interest in the relatively new field of "spintronics".

## References

1. C.F.Majkrzak, J.Kwo, M.Hong, Y.Yafet, D.Gibbs, C.L.Chien, and J.Bohr, Advances in Physics 40, 99 (1991).
2. M.R.Fitzsimmons, S.D.Bader, J.A.Borchers, G.P.Felcher, J.K.Furdyna, A.Hoffmann, J.B.Kortright, I.K.Schuller, T.C.Schulthess, S.K.Sinha, M.F.Toney, D.Weller, and S.Wolf, Journal of Magnetism and Magnetic Materials, in press.
3. K.V.O'Donovan, J.A.Borchers, C.F.Majkrzak, O.Hellwig, and E.E.Fullerton, Physical Review Letters 88, 672011(2002).
4. H.Kepa, G.Springholz, T.M.Giebultowicz, K.I.Goldman, C.F.Majkrzak, P.Kacman, J.Blinkowski, S.Holl, H.Krenn, and G.Bauer, Physical Review B, in press.

# Polarization Analysis of Thermal-Neutron Scattering*

R. M. Moon, T. Riste,† AND W. C. Koehler

*Solid State Division, Oak Ridge National Laboratory, Oak Ridge, Tennessee 37830*

(Received 30 December 1968)

A triple-axis neutron spectrometer with polarization-sensitive crystals on both the first and third axes is described. The calculation of polarized-neutron scattering cross sections is presented in a form particularly suited to apply to this instrument. Experimental results on nuclear incoherent scattering, paramagnetic scattering, Bragg scattering, and spin-wave scattering are presented to illustrate the possible applications of neutron-polarization analysis.

## I. INTRODUCTION

WE have added a new dimension to measurements of thermal-neutron scattering by constructing, at the Oak Ridge High-Flux Isotope Reactor, a triple-axis spectrometer with polarization-sensitive crystals on both the first and third axes. With this instrument the distribution of scattered neutrons from an initially monochromatic, polarized beam is measured as a

scattering $(++$ and $--)$. The theoretical quantities of greatest interest are the partial cross sections.

This is a different language than is customarily used by theoreticians in describing the scattering of polarized neutrons. The total cross section (summed over final spin states) and the final polarization are calculated as a function of the initial polarization. The polarization equation is a vector relationship giving the magnitude and direction of the final polarization. We measure

$$F^{\pm\pm} \propto \sum_{j=1}^{N} \left[ b_{s_j} \pm P_{s_j} \cos\phi_j \right] e^{iQu_j}$$

$$F^{\pm\mp} \propto \sum_{j=1}^{N} P_{s_j} \sin\phi_j \, e^{iQu_j}$$

$\vec{P}_i$

$\theta$

$\vec{k}_i$

$\vec{Q}$

z-axis

$M$

$\phi$

$\vec{k}_f$

d

D

$\theta$

$\vec{P}_f$

$$\vec{Q} \equiv \left| \vec{k}_f - \vec{k}_i \right|$$
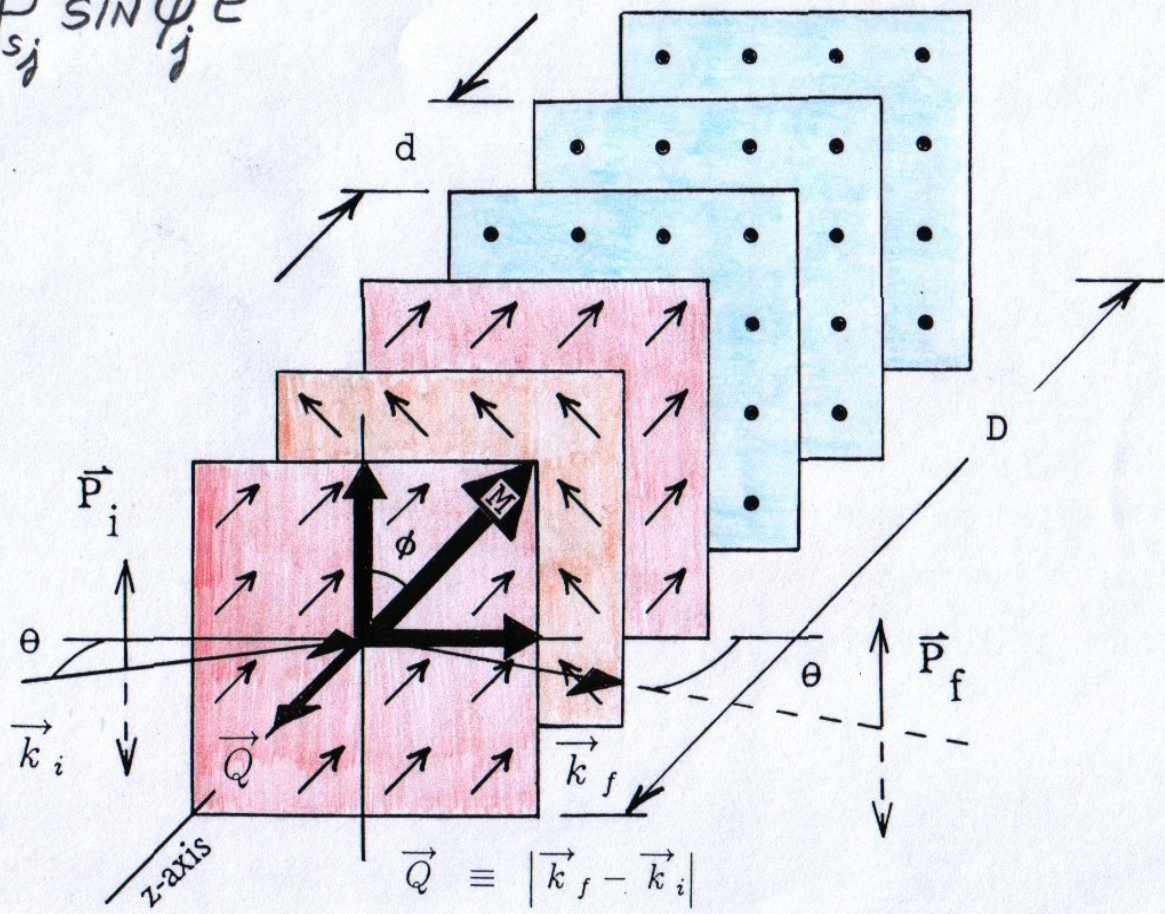
# SELECTION RULES FOR SCATTERING OF POLARIZED NEUTRONS BY MAGNETIC MOMENTS

- ONLY MAGNETIZATION COMPONENTS $\perp \vec{Q}$ GIVE RISE TO SCATTERING

- COHERENT NUCLEAR SCATTERING : ALL NSF

- NUCLEAR SPIN INCOHERENT

| FIELD AT SAMPLE | SF | NSF |
|---|---|---|
| $\vec{H} \parallel \vec{Q}$ | 2/3 | 1/3 |
| $\vec{H} \perp \vec{Q}$ | " | " |

- ANTIFERROMAGNET OR PARAMAGNET

| FIELD AT SAMPLE | SF | NSF |
|---|---|---|
| $\vec{H} \parallel \vec{Q}$ | 1 | 0 |
| $\vec{H} \perp \vec{Q}$ | 1/2 | 1/2 |

- SPIRAL MAGNETIC STRUCTURES WITH SINGLE DOMAIN OF ONE CHIRALITY :

$\vec{H} \parallel \vec{Q}$   $+ \rightarrow -$  OR  $- \rightarrow +$   SF ONLY,

DEPENDING ON WHETHER SPIRAL IS RIGHT- OR LEFT- HANDED

# Magnetic Neutron Scattering

Neutron: $\qquad$ $S = 1/2 ;$ $\qquad$ $\mu = 1.91\,\mu_N$

Scattering by atomic
magnetic moments: $\quad p = 0.54 \times S \times f\,(\sin\theta / \lambda) \times 10^{-12}\,cm$

*Magnetic and nuclear scattering amplitudes
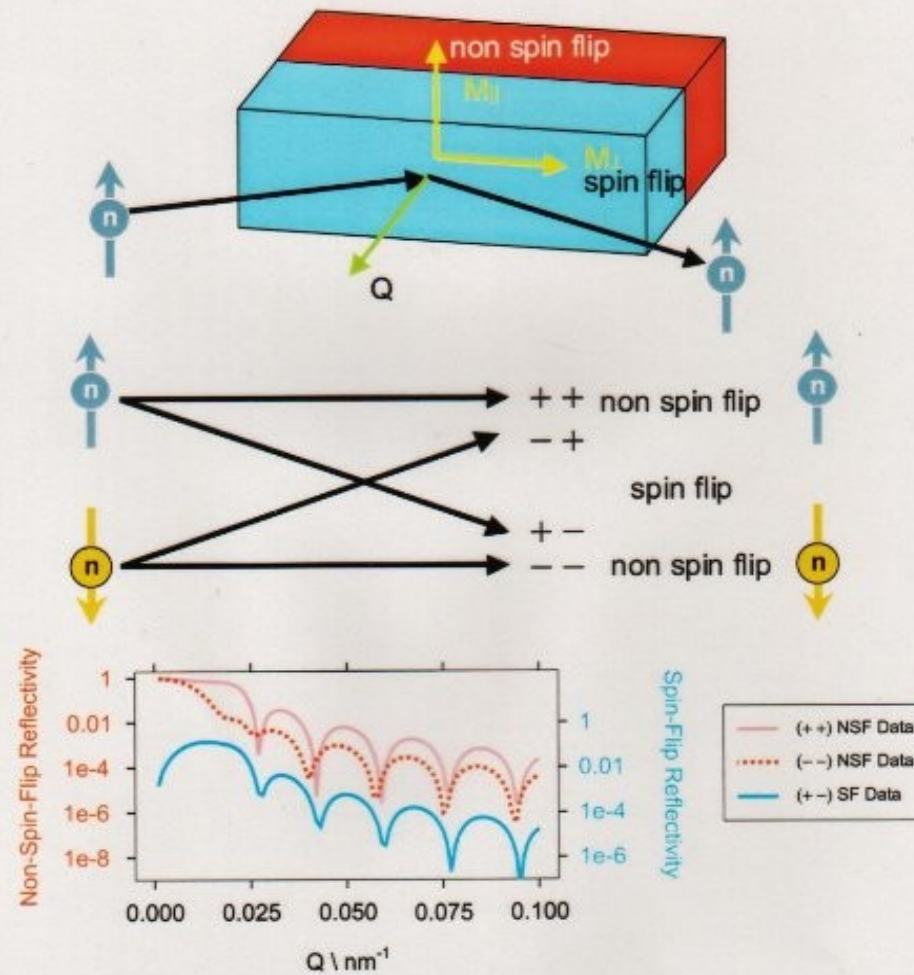are of similar magnitude*

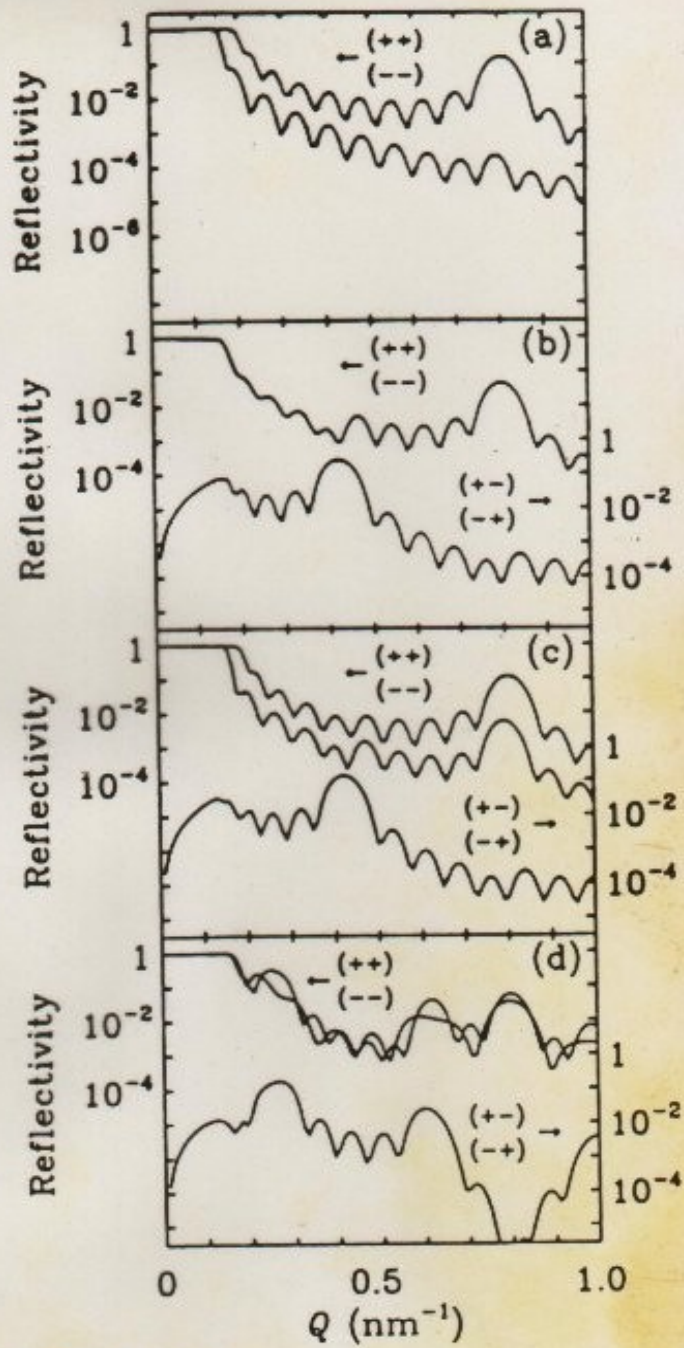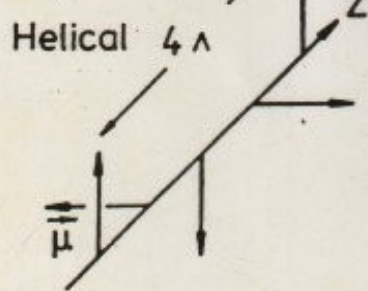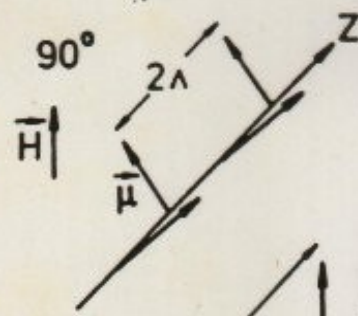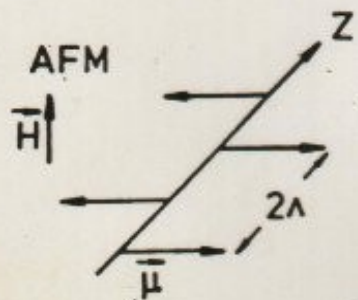## DIFFRACTION BY MAGNETIC CRYSTALS
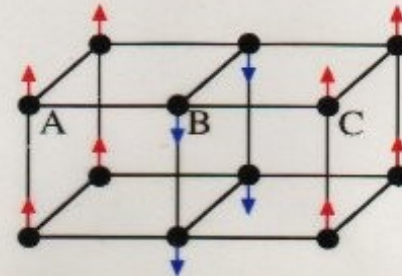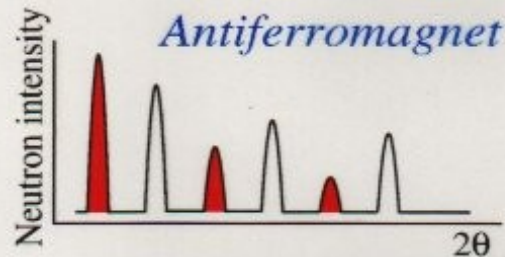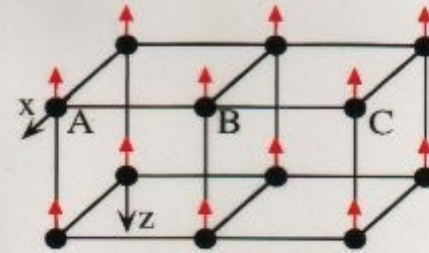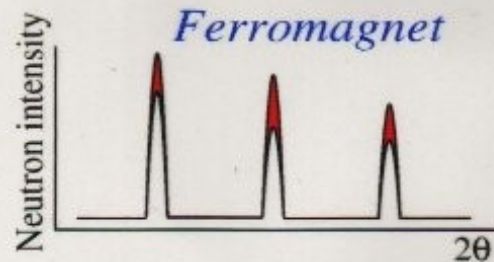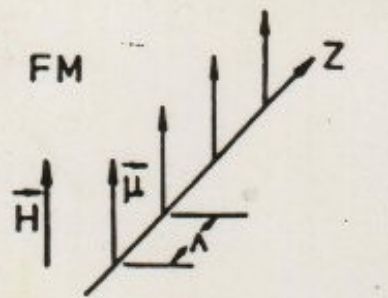


(from Julie Borchers)
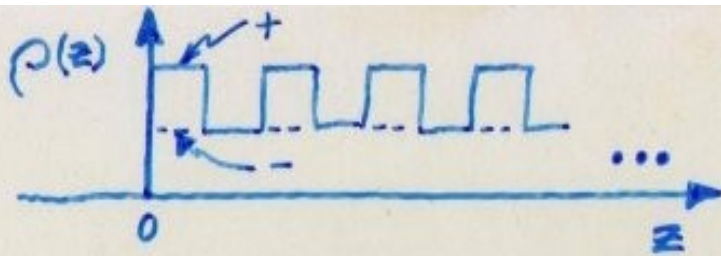
# Polarized Neutron Reflectometry
## at the NCNR NG-1 Reflectometer

Scattering experiment determines the correlation of magnetism at two depths separated by $d \sim 2\pi/Q$
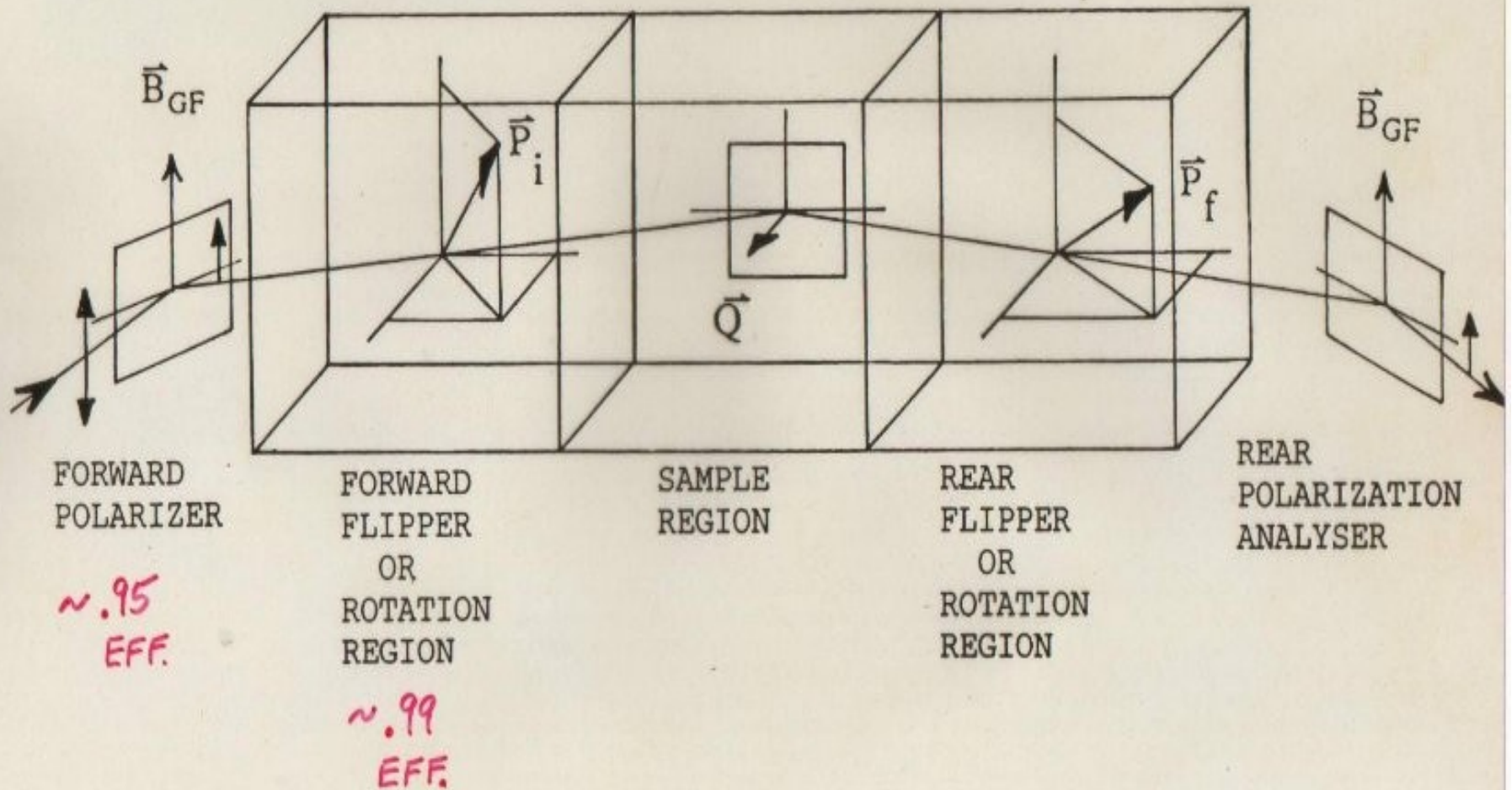


(from Julie Borchers)

FM

AFM

90°

Helical 4 Λ

(a)
← (++)
(−−)

(b)
← (++)
(−−)
(+−) →
(−+)

(c)
← (++)
(−−)
(+−) →
(−+)

(d)
← (++)
(−−)
(+−) →
(−+)

Reflectivity

$Q$ (nm$^{-1}$)

ANKNER, SCHREYER,
MAJKRZAK, ZABEL, et al.

$\rho(z)$

$|F_{\pm}|^2 \propto |N_b \pm N_p|^2$

$\vec{B}_{GF}$

$\vec{P}_i$

$\vec{Q}$

$\vec{P}_f$

$\vec{B}_{GF}$

FORWARD
POLARIZER

~.95
EFF.

FORWARD
FLIPPER
OR
ROTATION
REGION

~.99
EFF.

SAMPLE
REGION

REAR
FLIPPER
OR
ROTATION
REGION

REAR
POLARIZATION
ANALYSER

MEASURED ON BT-7
POLARIZED BEAM REFLECTOMETER
AT NIST

C.F. MAJKRZAK et al.

↑↓ INCIDENT / ↓ TRANSMITTED / ↑ REFLECTED

UNBROADENED TRANSMITTED BEAM

DISCARDED REFLECTED SPIN STATE

7.5 cm
5 cm
2.5 cm

100 PLATE CURVED STACK

○ UNPOLARIZED INCIDENT BEAM

- ~70.% TRANSMISSION OF ONE SPIN STATE
- WITH POLARIZING EFF. 95.%+
- OVER ANGULAR RANGE OF ~18. MINUTES @ $\lambda = 2.35$ Å

↓ "−" SPIN

↑ "+" SPIN

SINGLE PLATE Transmission

1.2 — 1.0 — 0.8 — 0.4 — 0.0

Q (Å⁻¹): 0.00   0.02   0.04   0.06   0.08   0.10

~ $3 \times Q_{c_{Ni}}$
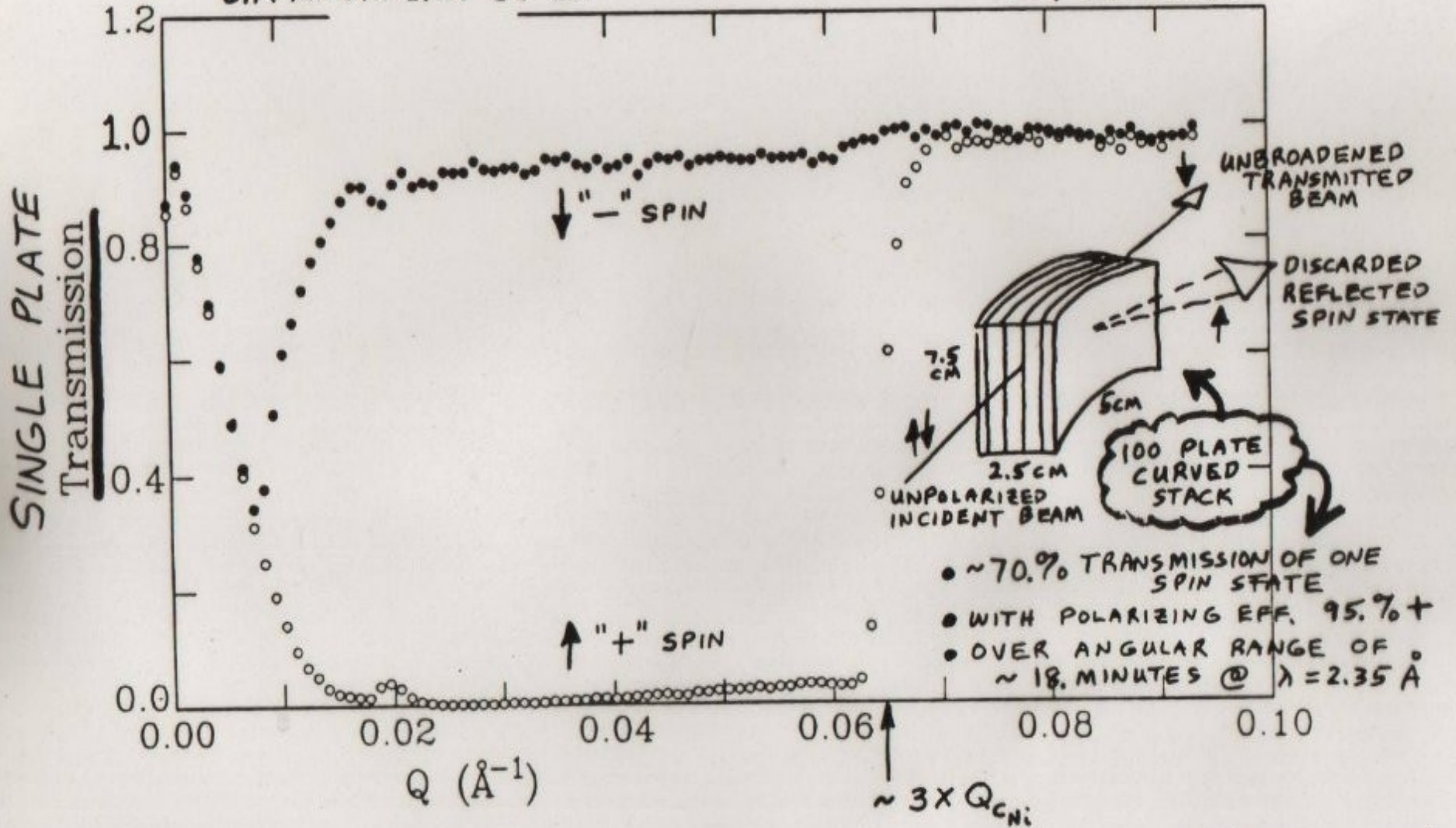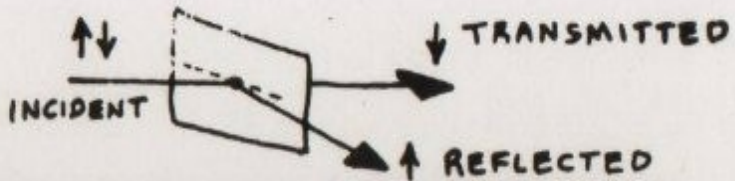
Fe/Si SUPERMIRROR POLARIZER IN TRANSMISSION (SINGLE CRYSTAL Si SUBSTRATE)
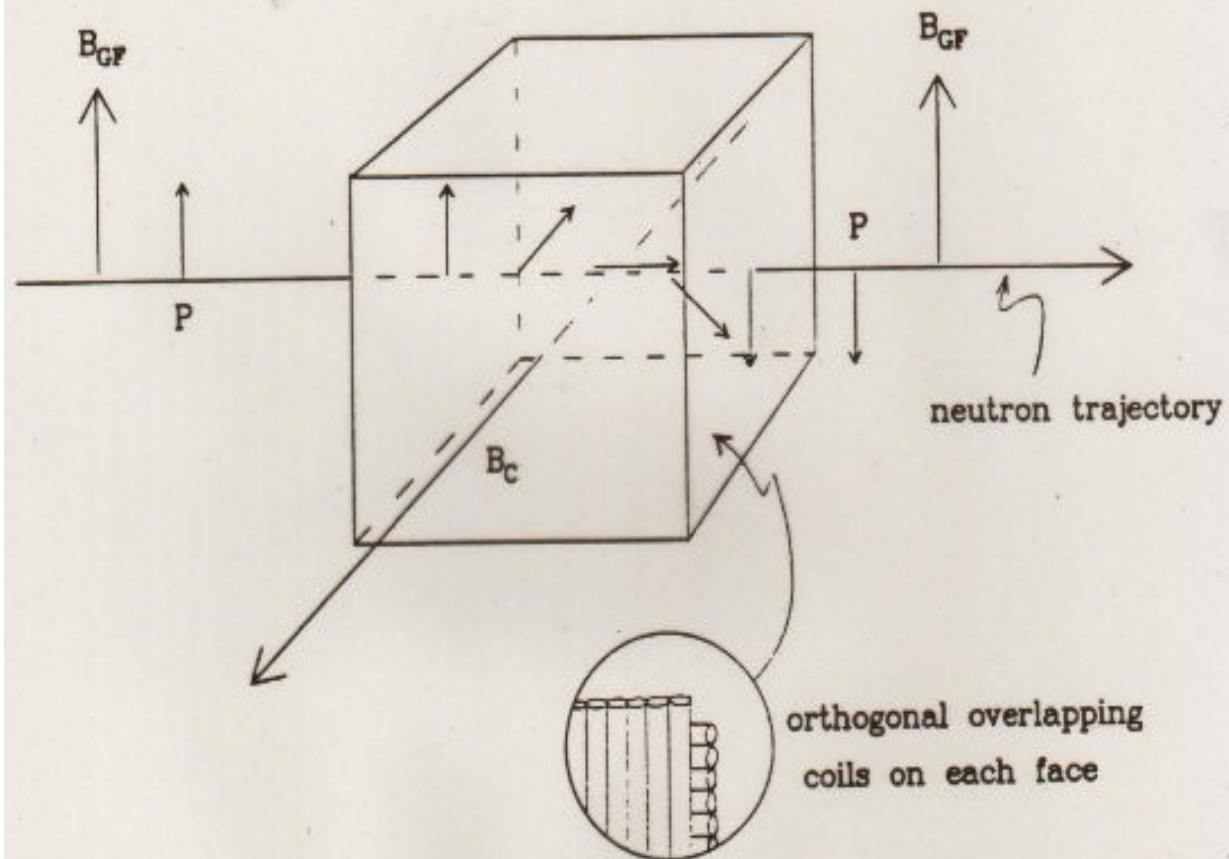(COATING MANUFACTURED BY OSMC COMPANY — J. WOOD)

**Fig. 5-2**

Figure 5-2. Cubic volume defined by three mutually orthogonal, intersecting solenoidal coils of square cross section within which a magnetic field $\vec{B}_c$ is created. Assuming sudden transitions across the coil boundaries, the neutron polarization will precess about the different field direction inside the coil as described in the text. Thus, the neutron polarization $\vec{P}$ can be rotated to any general orientation in space relative to the guide field $\vec{B}_{GF}$.

# Polarized Beam Reflectometer (PBR) at NIST
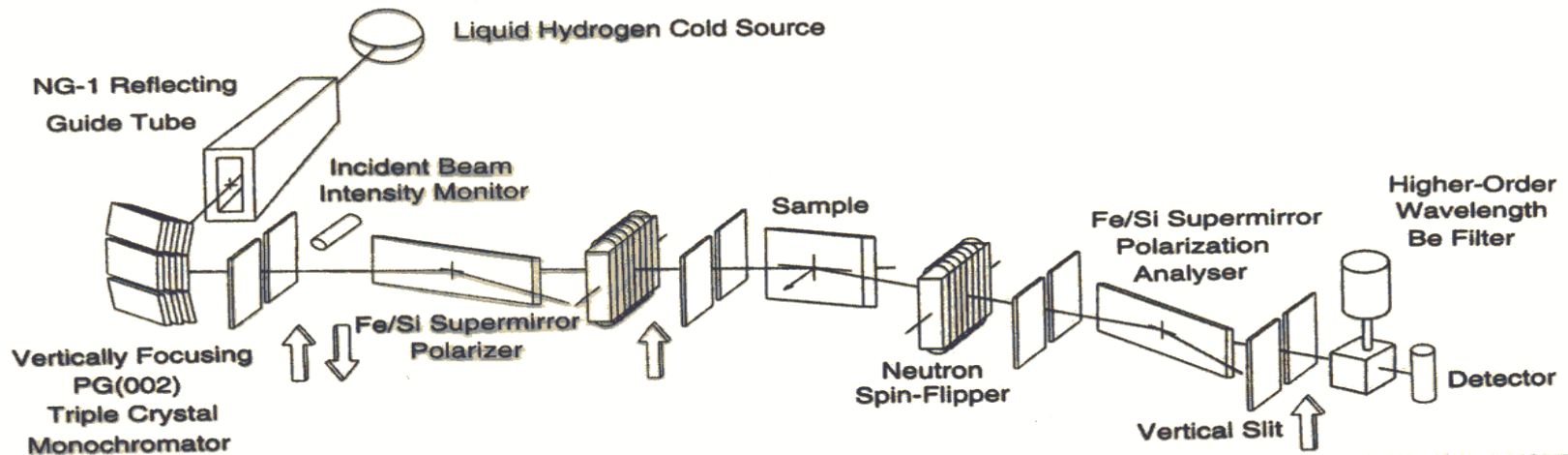
# NIST Vertical Sample, Polarized Neutron Reflectometer

The VREFL reflectometer uses a vertically focusing pyrolytic graphite monochromator to intercept the full height (15 cm) and width (6 cm) of the beam in the NG-1 guide and focuses it down to ~ 3 cm at the sample. Adjustable slits after the monochromator and in front of the sample, 1.5 m away, define the beam width and collimation.  Highly efficient (polarization > 98 %, and transmission of one spin state ~ 80 %) supermirror polarizers, shown in the photo below, may be inserted in the incident and reflected beams to provide full polarization analysis.  Overall instrumental flipping ratios of the order of 100 are routinely achieved.

| Instrument Specifications | |
| --- | --- |
| Wavelength, & resolution | 4.75 Å, 1.5 % $\Delta\lambda/\lambda$ |
| Q-resolution nearly constant | $\Delta Q/Q = 0.025$ |
| Flux at sample | $10^5$ n/cm$^2$-s typically |
| Minimum measurable reflectivity | $< 10^{-8}$ |

## TABLE 2: POLARIZING AND FLIPPING EFFICIENCY CORRECTIONS

$\sigma_{++}, \sigma_{--}, \sigma_{+-}$, and $\sigma_{-+}$ are defined as the NSF and SF reflectivities, respectively, corresponding to the sample.

$I^{off\ off}, I^{on\ on}, I^{off\ on}$, and $I^{on\ off}$ are defined as the intensities measured with front and rear flippers respectively, in "on" ($\pi$ rotation of the neutron spin) or "off" (no rotation) states.

F, R, f, and r are defined as the front and rear polarizer and front and rear flipper efficiencies, respectively.

---

The relationship between the intensities measured in the detector and the sample spin-dependent reflectivities are [28]

$$I^{off\ off}/\beta = \sigma_{++}(1+F)(1+R) \qquad I^{on\ off}/\beta = \sigma_{++}(1+R)[1+F(1-2f)]$$
$$+\sigma_{-+}(1-F)(1+R) \qquad\qquad +\sigma_{-+}(1+R)[1-F(1-2f)]$$
$$+\sigma_{--}(1-F)(1-R) \qquad\qquad +\sigma_{--}(1-R)[1-F(1-2f)]$$
$$+\sigma_{+-}(1+F)(1-R) \qquad\qquad +\sigma_{+-}(1-R)[1+F(1-2f)]$$

$$I^{off\ on}/\beta = \sigma_{++}(1+F)[1+R(1-2r)] \qquad I^{on\ on}/\beta = \sigma_{++}[1+F(1-2f)][1+R(1-2r)]$$
$$+\sigma_{-+}(1-F)[1+R(1-2r)] \qquad\qquad +\sigma_{-+}[1-F(1-2f)][1+R(1-2r)]$$
$$+\sigma_{--}(1-F)[1-R(1-2r)] \qquad\qquad +\sigma_{--}[1-F(1-2f)][1-R(1-2r)]$$
$$+\sigma_{+-}(1+F)[1-R(1-2r)] \qquad\qquad +\sigma_{+-}[1+F(1-2f)][1-R(1-2r)]$$

The spin-dependent reflectivities can be solved for from the measured intensities if the instrumental polarizing and flipping efficiencies and the constant $\beta$ are determined.

---

The constant $\beta$ is given by

$$2\beta = \frac{I_{NS}^{on\ on}\ I_{NS}^{off\ off} - I_{NS}^{on\ off}\ I_{NS}^{off\ on}}{I_{NS}^{on\ on} + I_{NS}^{off\ off} - I_{NS}^{on\ off} - I_{NS}^{off\ on}} \equiv \alpha$$
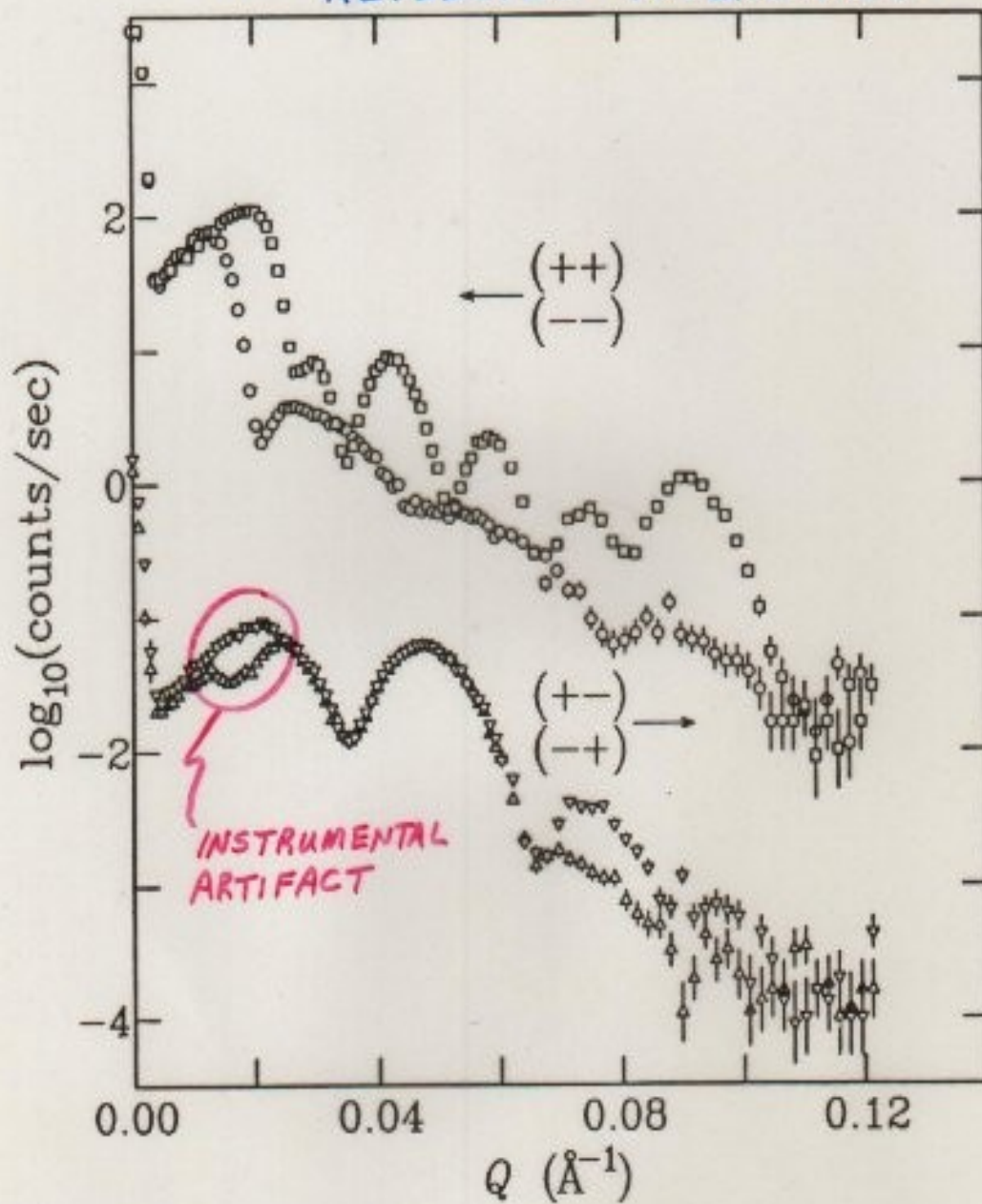
where the subscript "NS" signifies measurements at zero scattering angle with "no sample" in place. Also,

$$I_{NS}^{off\ off}/\alpha = FR + 1$$
$$I_{NS}^{on\ off}/\alpha = FR(1-2f) + 1$$
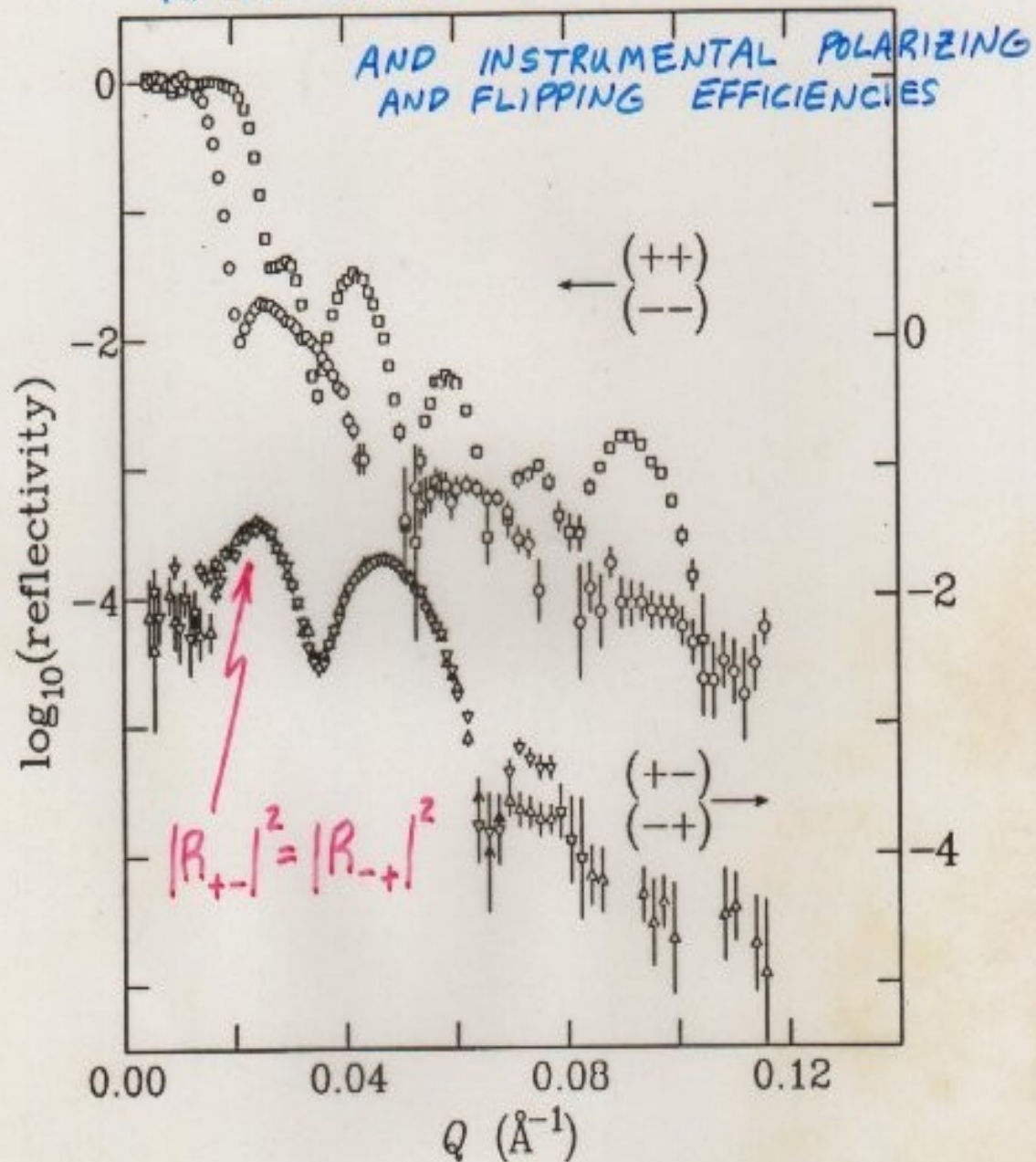$$I_{NS}^{off\ on}/\alpha = FR(1-2r) + 1$$

so that f, r, and the product F R can be determined.

---

If the sample is replaced with a "reference sample" (RS) which has $\sigma_{++} \neq \sigma_{--}$ and $\sigma_{+-} = \sigma_{-+} = 0$ ($\sigma_{++}$ and $\sigma_{--}$ need not be known), then F and R can be individually determined.

FeCr SUPERLATTICE : REFLECTIVITIES
AFTER CORRECTION FOR BEAM FOOTPRINT
AND INSTRUMENTAL POLARIZING
AND FLIPPING EFFICIENCIES

$\leftarrow \begin{pmatrix} ++ \\ -- \end{pmatrix}$

$\begin{pmatrix} +- \\ -+ \end{pmatrix} \rightarrow$

$|R_{+-}|^2 = |R_{-+}|^2$

$\log_{10}(\text{reflectivity})$

$Q \; (\text{Å}^{-1})$

# The Nobel Prize in Physics 2007

*This year's Nobel Prize in Physics is awarded to ALBERT FERT and PETER GRÜNBERG for their disco-very of Giant Magnetoresistance. Applications of this phenomenon have revolutionized techniques for retrieving data from hard disks. The discovery also plays a major role in various magnetic sensors as well as for the development of a new generation of electronics. The use of Giant Magnetoresistance can be regarded as one of the first major applications of nanotechnology.*

## Better read-out heads for pocket-size devices

Constantly diminishing electronics have become a matter of course in today's IT-world. The yearly addition to the market of ever more powerful and lighter computers is something we have all started to take for granted. In particular, hard disks have shrunk – the bulky box under your desk will soon be history when the same amount of data can just as easily be stored in a slender laptop. And with a music player in the pocket of each and everyone, few still stop to think about how many cds' worth of music its tiny hard disk can actually hold. Recently, the maximum storage capacity of hard disks for home use has soared to a terabyte (a thousand billion bytes).
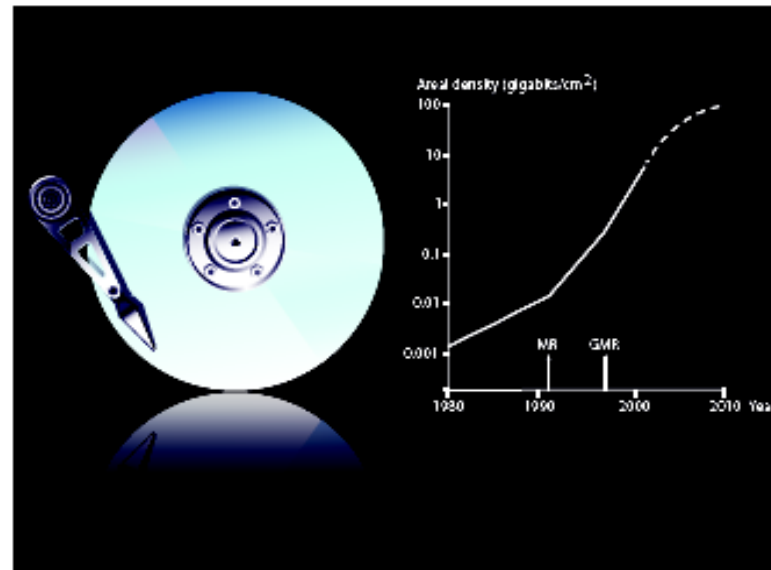


Diagrams showing the accelerating pace of miniaturization might give a false impression of simplicity – as if this development followed a law of nature. In actual fact, the ongoing IT-revolution depends on an intricate interplay between fundamental scientific progress and technical fine tuning. This is just what the Nobel Prize in Physics for the year 2007 is about.
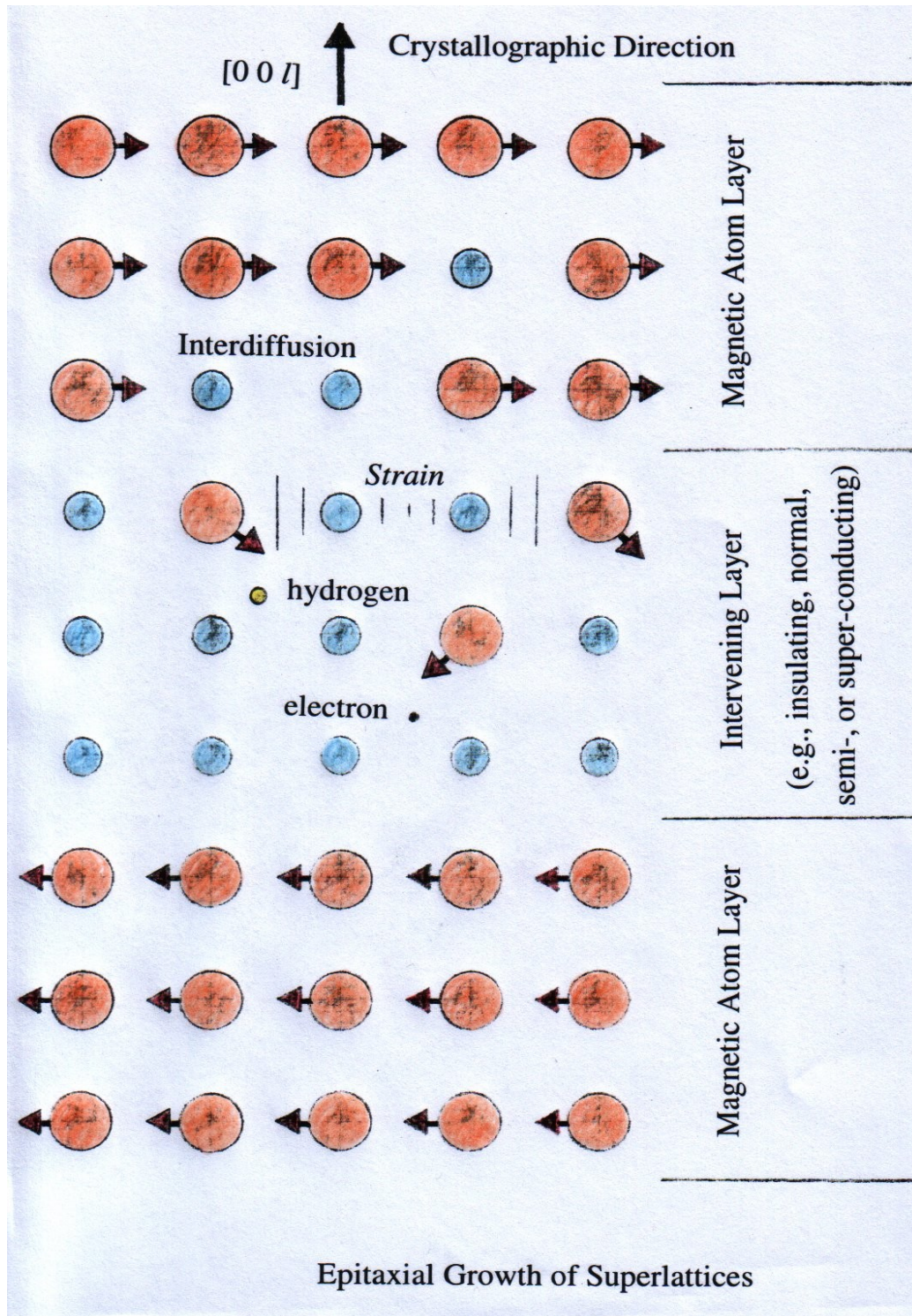
As recounted in the "Scientific Background" material referred to on the left side of the page, prior to the discovery of the GMR effect by Gruenberg, polarized neutron diffraction studies of magnetic superlattices revealed an unambiguous coupling between magnetic layers across intervening nonmagnetic spacers. The interlayer coupling (IEC) observed in this neutron diffraction work was explained in terms of long-range exchange interactions, for example, the RKKY (Ruderman Kittel Kasuya Yosida) interaction. Interestingly, the underlying mechanism responsible for GMR was thus known about before the effect itself was discovered! Much of the original neutron diffraction work was performed at the NIST (then NBS) neutron scattering facility by scientists including James Rhyne, Ross Erwin, and Julie Borchers, some of whom continue related forefront research today at the NCNR.
This is an example of the continuing importance of neutron scatttering as a fundamental probe of condensed matter.

Epitaxial Growth of Superlattices

$$\vec{Q} = \vec{k}_f - \vec{k}_i$$

[001]

$\vec{k}_i$     $\vec{k}_f$

A

(0002)

B

$N_{Gd}$

A

[001]

A

(0002)

B

$N_Y$

A

HEXAGONAL CLOSE-PACKED

$\lambda_{SL}$

$$\left[ Gd_{N_{Gd}} - Y_{N_Y} \right]_M$$
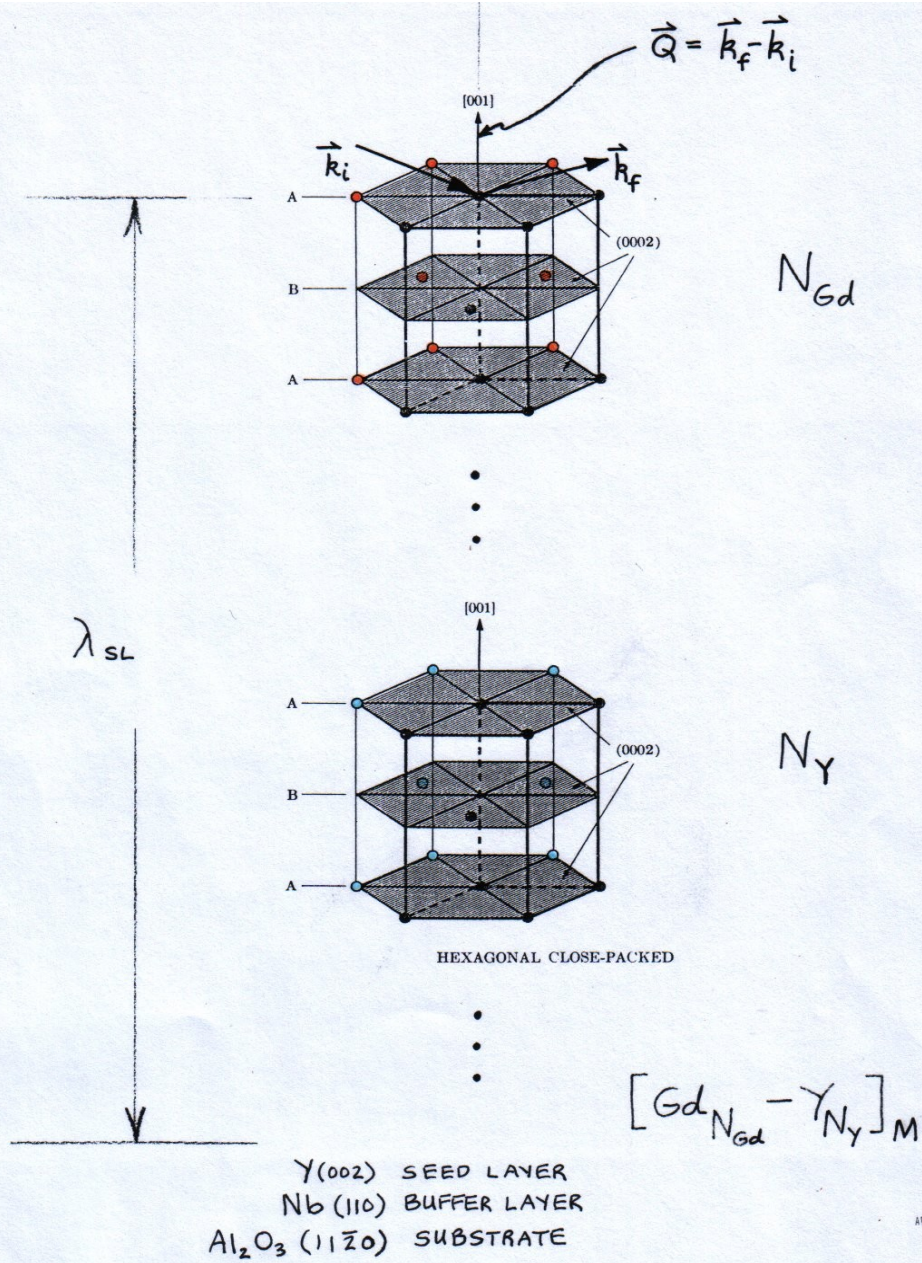
Y (002) SEED LAYER
Nb (110) BUFFER LAYER
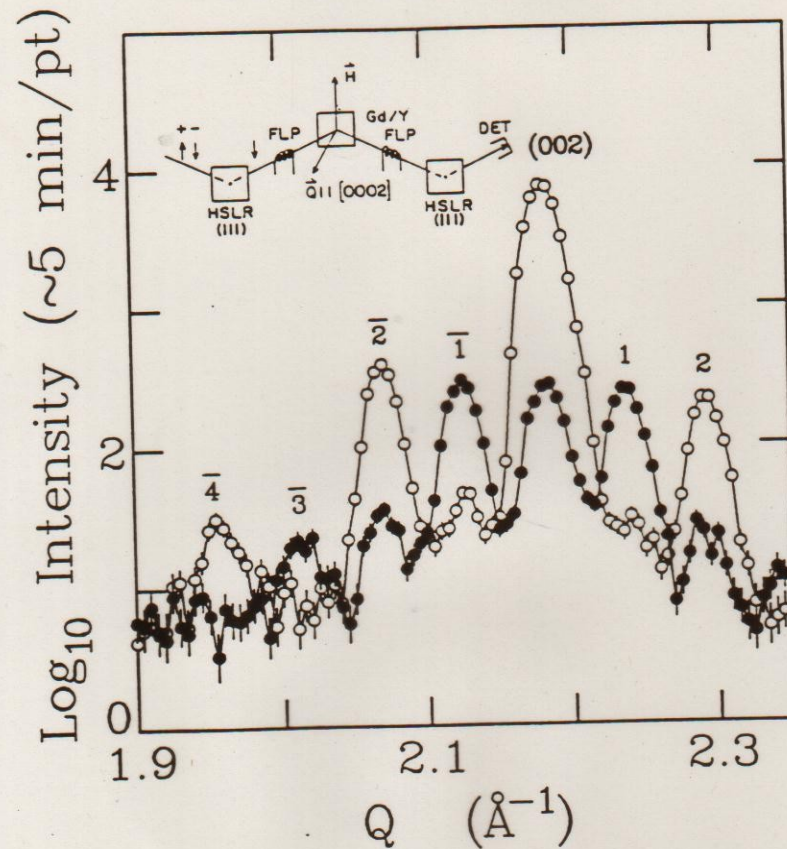Al$_2$O$_3$ (11$\bar{2}$0) SUBSTRATE

Fig. 7-1

Figure 7-1. NSF (open circles) and SF (filled circles) scattering from a [$Gd_{10}$ - $Y_{10}$] superlattice as described in the text. The data have not been corrected for instrumental polarizing and flipping efficiencies (the SF scattering at the (002) position is predominantly, if not entirely, instrumental in origin). The SF scattering which appears at values of Q corresponding to a doubling of the chemical bilayer spacing (odd-numbered satellites) is consistent with an antiferromagnetic alignment (for an applied field approaching zero) of neighboring ferromagnetic Gd layers as depicted schematically in Figure 7-2. (After Majkrzak et al. (1986)).
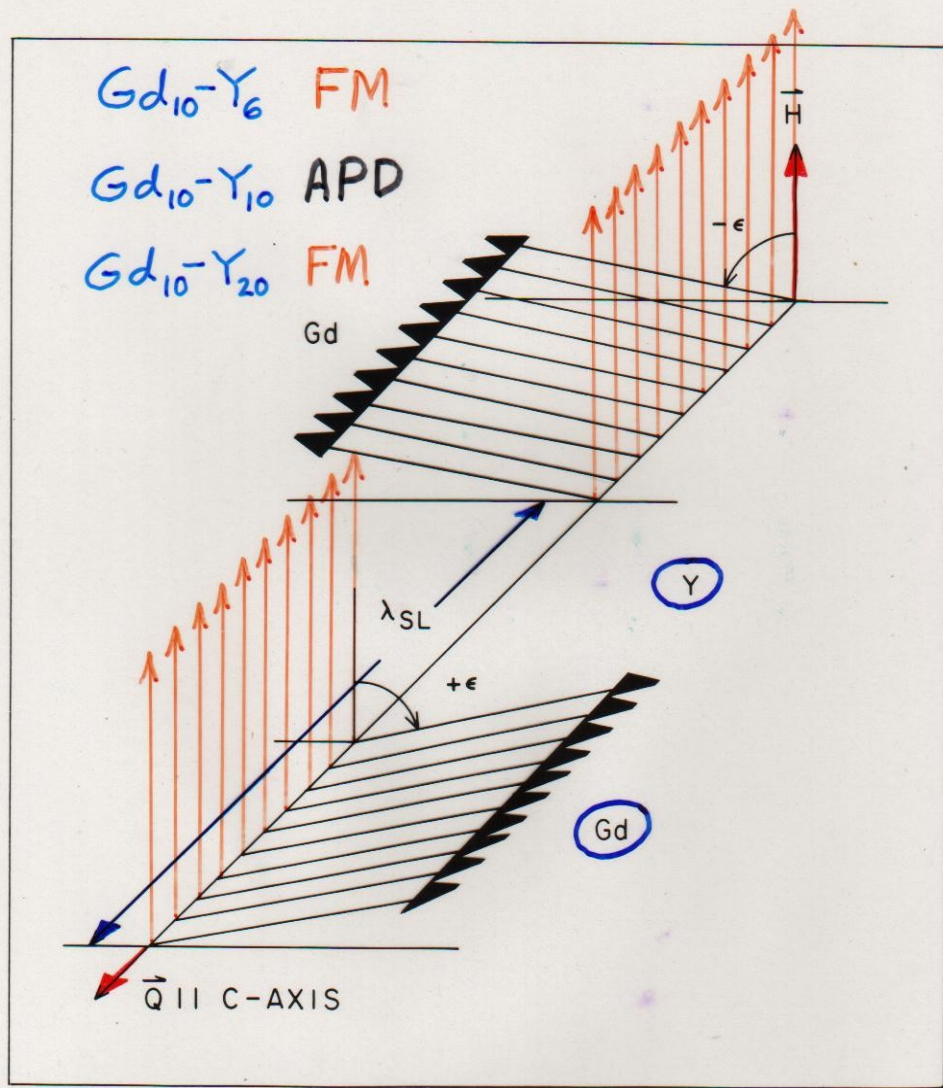
● n-diffr. meas.

Gd in Y,  Range Function,  qmax=.28*2pi/c
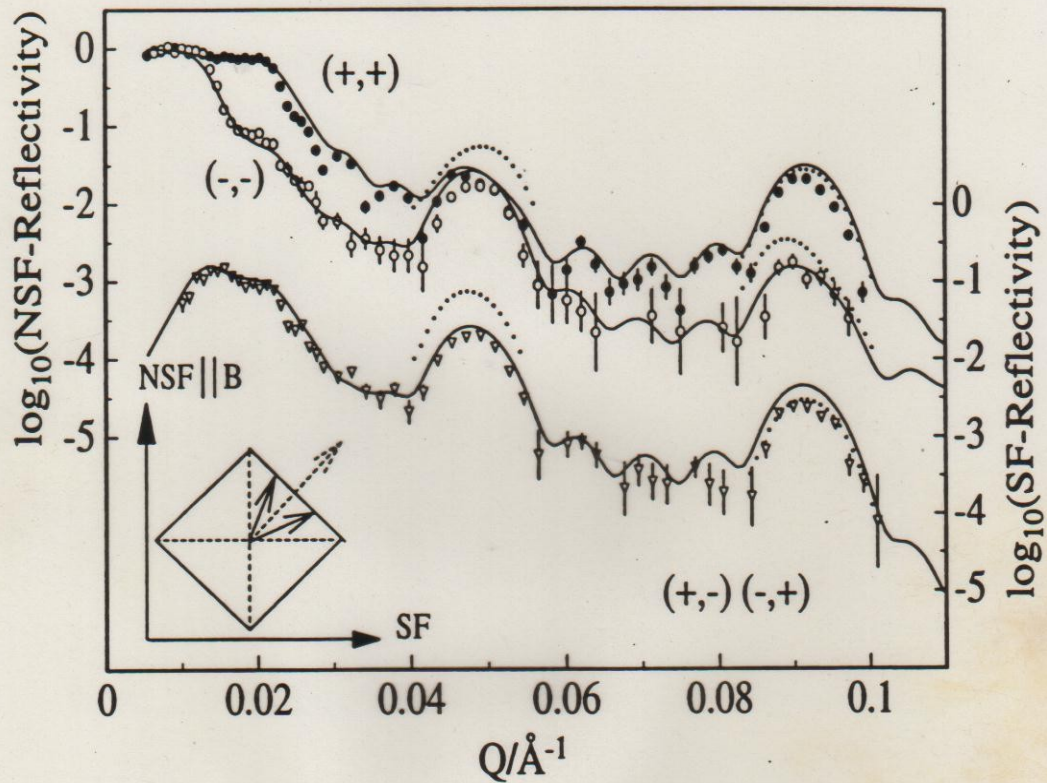
number of Y atomic layers inbetween
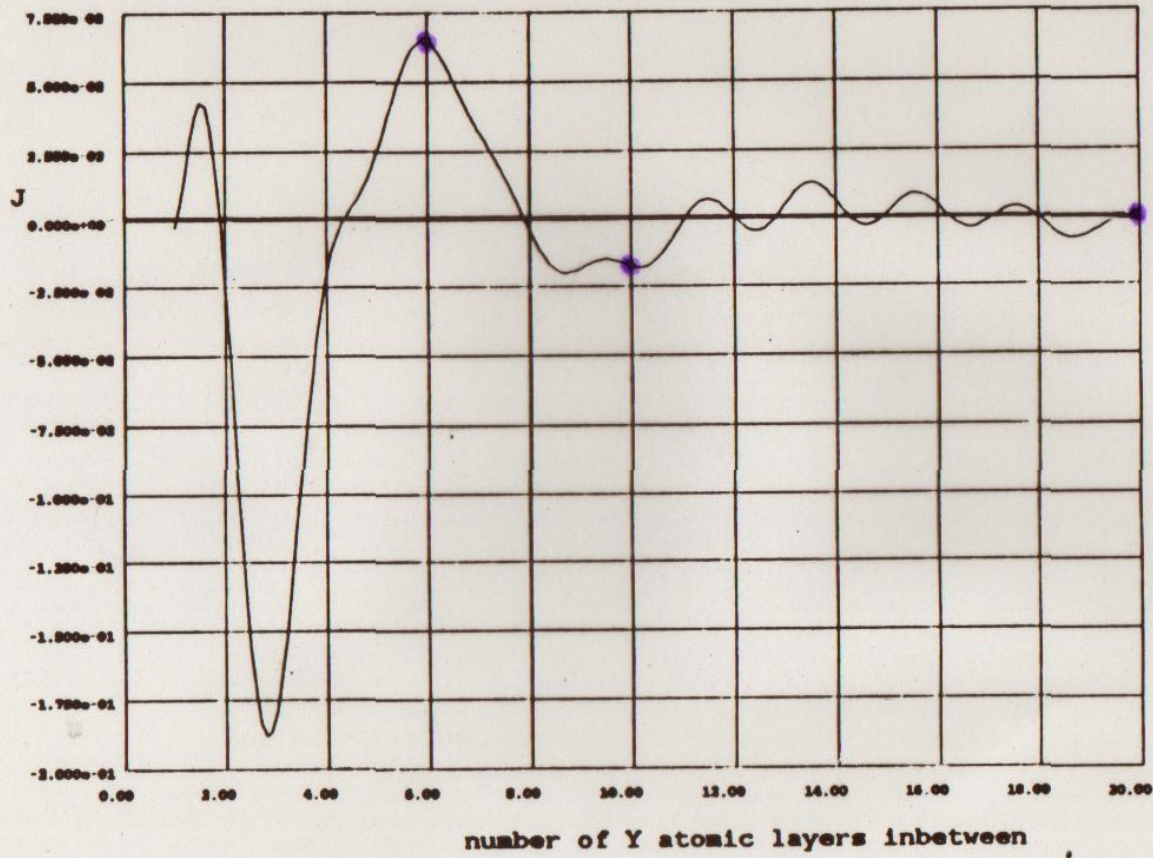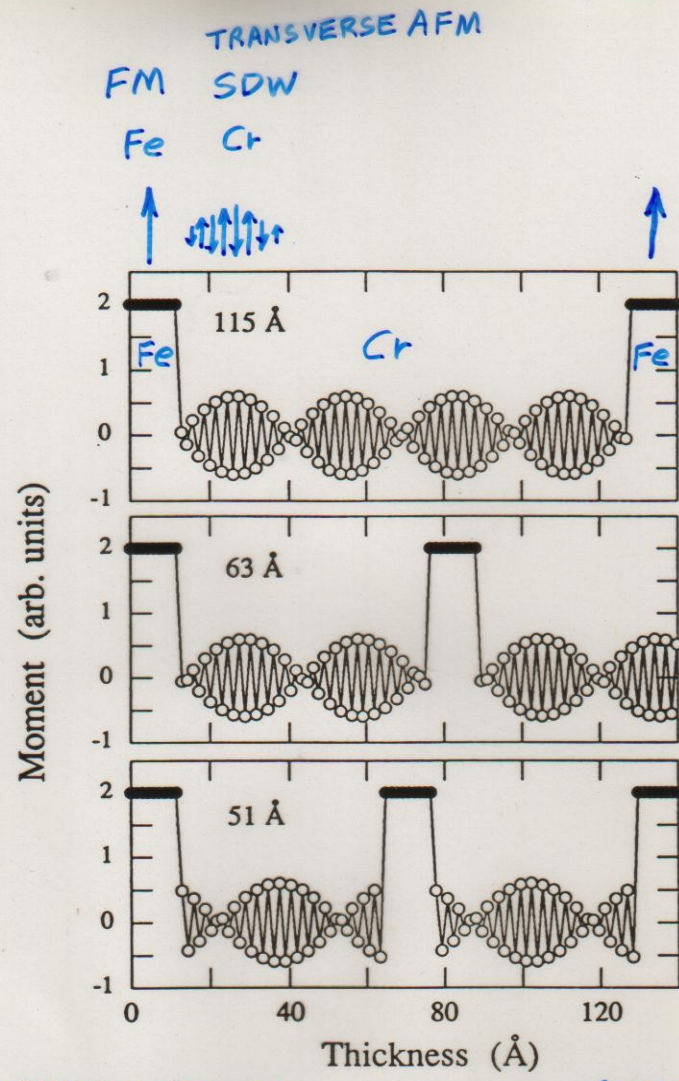
Figure 3

Fe/Cr SUPERLATTICES (GMR)

FULLERTON, BADER, & ROBERTSON

SCHREYER, ZEIDLER, ZABEL, ANKNER, MAJKRZAK, SCHÄFER, & GRÜNBERG, THIS CONFERENCE

NON COLLINEAR Fe/Cr (001)

..... $90° \not\!\!\!\triangleleft$

—— $50° \not\!\!\!\triangleleft$

$$E = -J_1 \frac{\vec{M}_1 \cdot \vec{M}_2}{|\vec{M}_1||\vec{M}_2|} - J_2 \left( \frac{\vec{M}_1 \cdot \vec{M}_2}{|\vec{M}_1||\vec{M}_2|} \right)^2$$

EXCHANGE COUPLING — BILINEAR — BIQUADRATIC

A. Schreyer et al.

Materials Science and Engineering Laboratory
NIST Center for Neutron Research

NIST
National Institute of
Standards and Technology

Home          Instruments          Science          Experiments          SiteMap
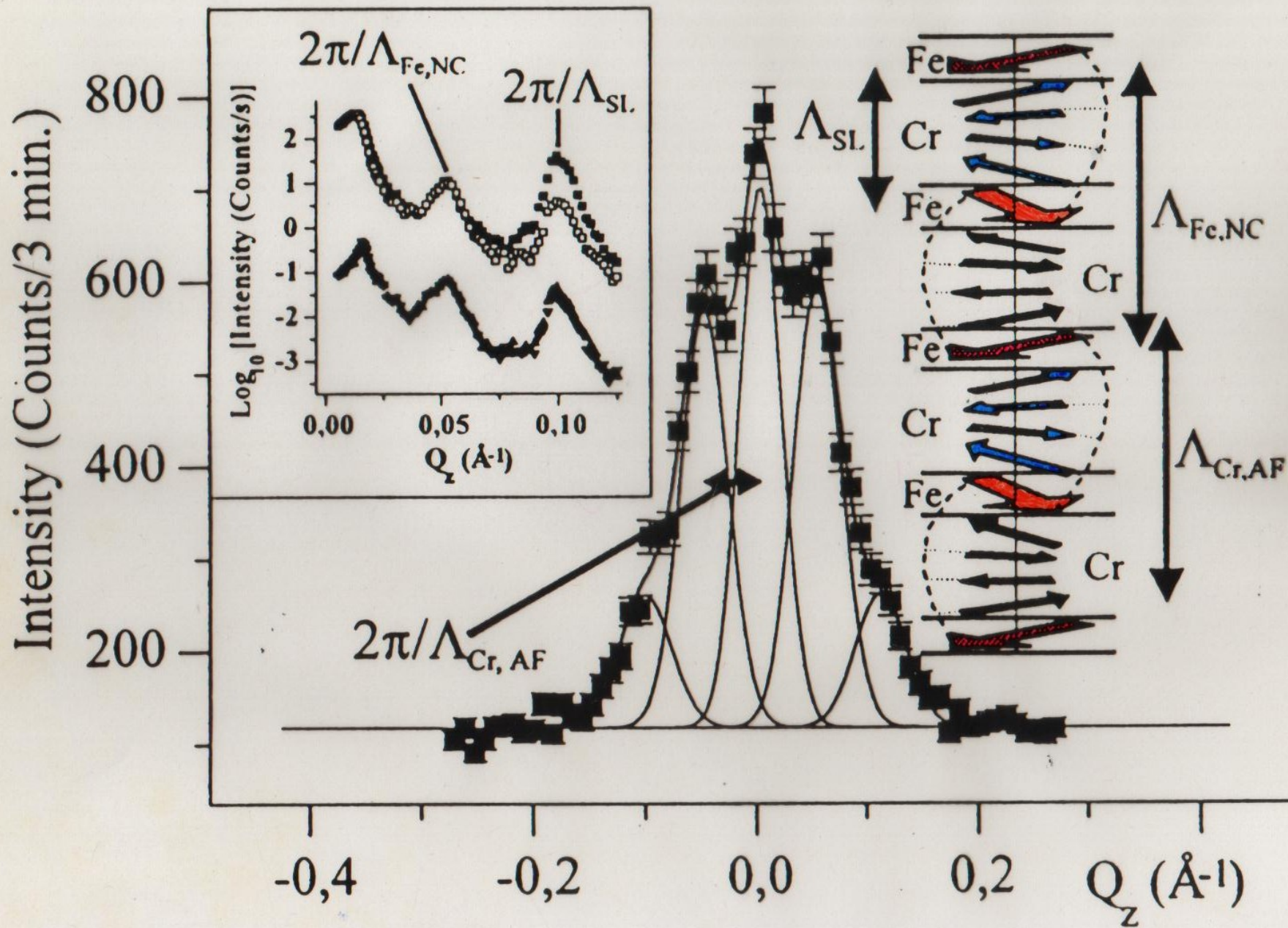
# Magnetic Semiconductor Superlattices

Currently a great deal of attention is being focused on spintronics, a new area of solid-state electronics. In spintronics not only the electric current but also its spin state is controlled. Spin valves and spin injectors are the first practical applications of spintronics. Further progress in developing new devices hinges critically on the availability of suitable materials. Such materials need to be ?good? semiconductors, easy to integrate in typical integrated circuits, and their electronic properties should exhibit strong sensitivity to the carrier?s spin, ferromagnetism being an especially desirable property.

EuS is one of the very few natural ferromagnetic (F M) semiconductors. Since it becomes F M at a low temperature ($T_c$ = 16.6 K) it is an unlikely choice for applications. However, studying the properties of heterostructures made on its base may give an important insight into fundamental processes taking place in all classes of materials under consideration.

GaMnAs is a man-made F M semiconductor. It is an example of a diluted magnetic semiconductor (D M S) in which a fraction of nonmagnetic cations (Ga) is substituted with magnetic ions (Mn). Such a material can readily be incorporated into modern GaAs-based semiconductor devices. Its $T_c$ is still below room temperature, but this limitation may be lifted in other materials of this class (Refer to Reference 1).

Interlayer exchange coupling (I E C) in superlattices (S L), composed of ferromagnetic and nonmagnetic layers, is a crucial element of all spin-valve type devices that utilize the giant magnetoresistance effect. In metallic S L's currently being used, conduction electrons transfer the interlayer interactions through nonmagnetic spacers (Refer to Reference 2). Here we address the question whether I E C phenomena are possible in all-semiconductor superlattices, like EuS/PbS and GaMnAs/GaAs, where the carrier concentrations are many orders of magnitude lower than in metals.

The nonmagnetic spacer in EuS/PbS S L's is a narrow gap semiconductor with electron concentration of the order of $10^{17}$ cm$^{-3}$ to $10^{18}$ cm$^{-3}$. For thin PbS layers ($d_{PbS}$ < 70 Å) neutron reflectivity spectra, shown in Figure 1, have revealed a pronounced maximum of magnetic origin at the position corresponding to the doubled structural S L periodicity, thus indicating the existence of antiferromagnetic (A F M) interlayer arrangements (Refer to Reference 3).
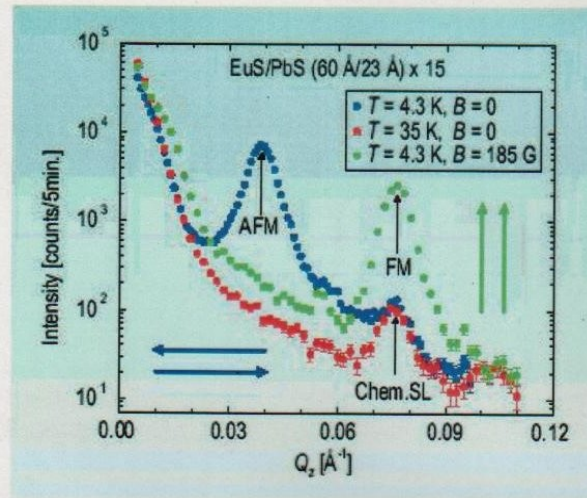
FIGURE 1. Unpolarized neutron reflectivity spectra for EuS/PbS S L with thin (23 Å) PbS spacer. Antiferromagnetic interlayer exchange coupling below $T_c$ and at zero external field is clearly visible (blue curve). Applying a strong enough magnetic field (185 G in this case) parallel to the S L surface forces all the EuS layer?s magnetizations to ferromagnetic configuration (green curve). Above $T_c$ the system is nonmagnetic, the only Bragg peak comes from the chemical S L periodicity.

For much thicker PbS spacers ($d_{PbS} > 120$ Å) the only magnetic peaks visible in the reflectivity profiles, see example in Figure 2, coincide with the chemical ones, thus leading to the conclusion that the magnetization vectors in adjacent EuS layers are parallel, which indicates F M I E C.
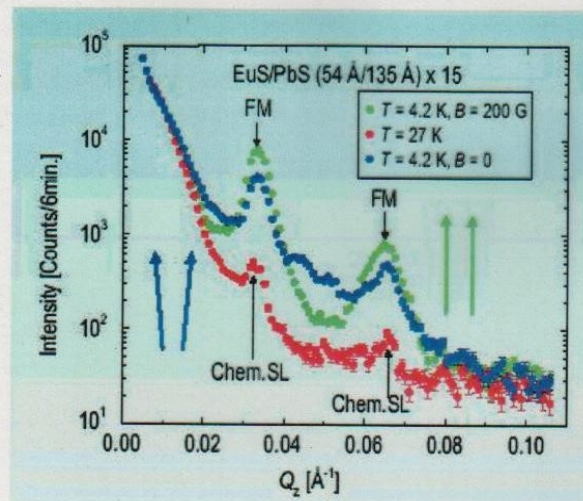
FIGURE 2. The sample with thick (135 Å) PbS layers is almost ferromagnetically coupled. Application of an external magnetic field enhances the F M Bragg peaks and lowers the intensity between them (at the A F M peak position).

In the intermediate PbS thickness range (70 Å $< d_{PbS} <$ 120 Å), both A F M and F M peaks are present. Polarized neutron analysis of these maxima gives evidence that the magnetization vectors of adjacent EuS layers are not colinear. Hence, the I E C found in EuS/PbS S L's has an oscillatory character similar to that occurring in metallic S L's, although the oscillation period is much longer than the one in metallic systems.

In order to confirm that the free carriers, present in the PbS layer in such a small amount, are the cause of the observed oscillatory I E C, a series of analogous measurements have been carried out on EuS/YbSe S L's. The structure and lattice constant of YbSe are the same as those of PbS. In contrast to PbS, YbSe is a semi-insulator with a negligible carrier concentration. Neutron reflectivity profiles have shown no evidence of any interlayer coupling in the all investigated samples. That finding, together with the oscillatory character of coupling in S L's with PbS spacer, strongly points to the leading role of PbS free electrons in providing the necessary I E C mechanism, similar to that discovered in metallic multilayers.

Ferromagnetic ordering in GaMnAs is carrier (holes) induced; the Mn atoms, apart from being the magnetic element in the system, act also as acceptors providing the holes responsible for transferring exchange interactions between them. The details of the magnetic ordering, in particular its range, are still being disputed.

To address the latter issue, polarized neutron reflectometry has been performed on a number of GaMnAs/GaAs superlattices. Figure 3 shows an example of the obtained reflectivity profile in the vicinity of the first S L Bragg peak, for one of the samples. The very presence of the magnetic contribution to the structural S L Bragg peak is a strong confirmation of the F M I E C between consecutive GaMnAs layers. The absence of any spin-flip scattering shows that the sample is in a one-domain state, i.e., the F M ordering in GaMnAs is long range, and the sample is spontaneously saturated. The peak in (--) cross section, and its absence in the (++), is proof that the magnetization is directed oppositely to the external magnetic guide field, hence the long range ordering has formed spontaneously, without the influence of the external field. More details can be found in Reference 4.
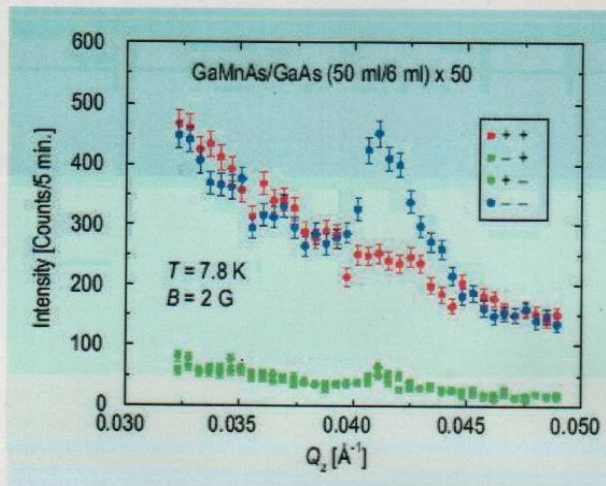
FIGURE 3. Polarized neutron reflectivity spectra for GaMnAs/GaAs superlattice.

References

[1] T. Dietl, H. Ohno, F. Matsukura, J. Cibert, D. Ferrand, Science 287,1018 (2000).

[2] P. Bruno, Phys. Rev. B52, 411 (1995).

[3] H. Kepa, J. Kutner-Pielaszek, J. Blinowski, A. Twardowski, C. F. Majkrzak, T. Story, P. Kacman, R. R. Galazka, K. Ha, H. J. M. Swagten, W. J. M de Jonge, A. Yu. Sipatov, V. Volobuev, T. M. Giebultowicz, Europhys. Lett. 56, 54 (2001).

[4] H. Kepa, J. Kutner-Pielaszek, A. Twardowski, C. F. Majkrzak, J. Sadowski, T. Story, T. M. Giebultowicz, Phys. Rev. B64, 121302 (2001).

Authors

A. Yu. Sipatov, V. Volobuev
Kharkov State Polytechnical University
Kharkov, Ukraine

H. Kepa, J. Kutner-Pielaszek, A. Twardowski
Institute of Experimental Physics
Warsaw University
Warsaw, Poland

T. Story, J. Sadowski
Institute of Physics
Polish Academy of Sciences
Warsaw, Poland

# Pinpointing Chiral Structures with Front/Back Polarized Neutron Reflectometry

K. V. O'Donovan, J. A. Borchers, and C. F. Majkrzak
NIST Center for Neutron Research
National Institute of Standards and Technology
Gaithersburg, MD 20899-8562

O. Hellwig, E. E. Fullerton
IBM Almaden Research Facility
San Jose, CA 95120-6001

**W**e have developed a new method of using polarized neutron reflectometry (PNR) to extract the structure of buried magnetic spirals in magnetic films. This technique improves upon earlier methods by being particularly sensitive to the presence of magnetic twists vis-à-vis structures in which the magnetization direction does not vary appreciably. Tracking the formation and growth of twists may solve a number of puzzles that hamper the development of magnetic thin film devices.

In collaboration with IBM scientists, we have applied the technique to a thin-film exchange-spring magnet and confirmed that the results may violate the current theory regarding the behavior of such magnets. It has been predicted that exchange-spring magnets, comprised of soft and hard ferromagnets in close proximity, are a composite that has a strong moment and does not readily demagnetize [1]. Therefore, exchange-spring magnets should give industry the ability to make much smaller permanent magnets for use in the magnetic recording devices, and elsewhere. As a side effect, when a small external magnetic field is opposed to that of the magnet, the portion of the soft ferromagnet farthest from the hard ferromagnet may twist into alignment with the field. When the field is removed, the soft ferromagnet untwists. The film provided by IBM consists of the hard ferromagnet $Fe_{55}Pt_{45}$ topped by the soft ferromagnet $Ni_{80}Fe_{20}$ [2].

Figure 1 shows a simplified diagram of the behavior predicted by current theories [1]. A magnetic field of 0.890 T, provided by an electromagnet, is sufficient to align both the soft and the hard layers of our exchange-spring magnet, as shown on the left. When a modest reverse field (on the order of 0.025 T) is applied to the exchange spring magnet, only the top of the soft layer will realign with the magnetic field. The hard layer remains pinned in the original direction, and a continuous twist is induced in the soft layer, as the direction of magnetization changes smoothly between the reverse field direction to the aligning field direction.

Although there are many alternatives to PNR to measure the magnetization, typically they measure only the average orientation of the magnetic spins, and cannot readily distinguish a spiral from a structure in which all the spins are canted with respect to an external field. PNR can extract the
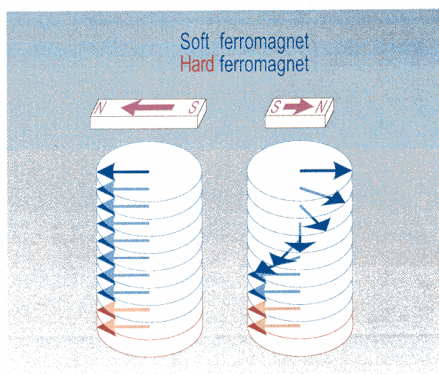


FIGURE 1. Model for field behavior of exchange-spring magnets. On the left the magnet has been aligned by a large external magnetic field. On the right a smaller field opposed to the first field causes a twist to form in the soft ferromagnet, while the hard ferromagnet remains aligned.

depth-dependence of the magnetic and chemical structure. We have studied the sample over a wide range of external magnetic fields, and can track the development of the spiral with field [3].

A PNR experiment begins with neutrons whose magnetic moments are aligned parallel (+) or opposite (–) to the external magnetic field. When the magnetization of the sample is perpendicular to this magnetic field, the neutron moment precesses as it interacts with the sample. When this happens the spin-flip (SF) reflectivities $R^{+-}$ and $R^{-+}$ are strong. If the magnetization of the sample is parallel to the external magnetic field, no precession occurs, but the non-spin-flip (NSF) reflectivities $R^{++}$ and $R^{--}$ will differ. The NSF reflectivities also provide information about the chemical structure of the film.

Our new modification of the PNR method greatly enhances the contrast between colinear and certain non-colinear magnetic structures [4]. We first measure the reflectivity with neutrons glancing off the front surface of the material, and then repeat with neutrons glancing off the back surface. The experiment is akin to holding the plane of the film up to a "magnetic mirror" to see whether the mirror image is the same as the original structure. In a colinear structure, all the spins are aligned along a common direction, and the mirror image is very much like the original structure.
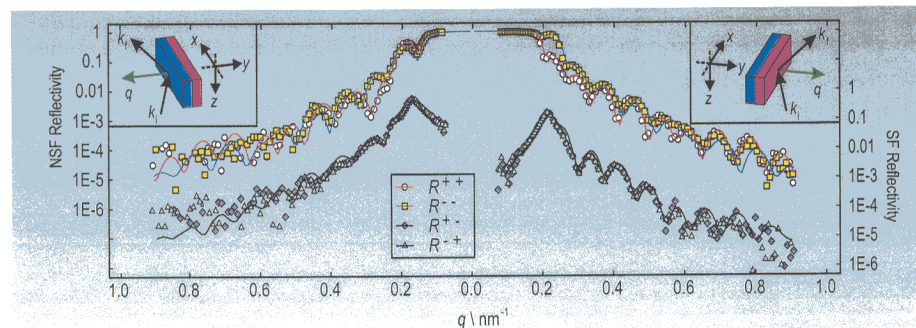


FIGURE 2. Reflectivity of a $Ni_{80}Fe_{20}|Fe_{55}Pt_{45}$ bilayer. The front reflectivity is plotted on the right while the back reflectivity is plotted on the left. The SF reflectivities $R^{+-}$ and $R^{-+}$ are plotted against the right ordinate axis. The NSF reflectivities $R^{++}$ and $R^{--}$ are plotted against the left ordinate axis.

But the mirror image of a magnetic twist to the right is a magnetic twist to the left. Therefore, if the front and back reflectivities are significantly different, we can deduce the presence of a spiral. Fitting the data confirms the spiral's existence.

Figure 2 shows data collected at 0.026 T after aligning in -0.89 T. Fits to the data are shown as solid lines. The data from the front reflectivity are shown on the right, and the data from the back reflectivity are shown on the left. The spin-flip (SF) reflectivities $R^{+-}$ and $R^{-+}$ are plotted against the right-hand axis, which have been shifted relative to the NSF reflectivities $R^{++}$ and $R^{--}$ plotted against the left axis. At $q = 0.2$ nm$^{-1}$, there is a splitting in the front NSF reflectivity that is much more pronounced than that of the back reflectivity at the same $q$. This is a hallmark of the spiral structure.

Figure 3 shows the magnetic structure that gives the excellent fit to the data plotted in Fig. 2. The location of the hard/soft interface is marked in Fig. 3. Surprisingly, we discover the spiral invades the hard ferromagnet even at extremely low fields. Current theory predicts that when this occurs, the soft ferromagnet will not be able to untwist fully. Yet, other magnetic studies show that our exchange-spring magnet does untwist when this field is removed. Thus, our PNR measurements have identified a shortcoming of current theory.

With this new technique, NIST is now able to better characterize the magnetic properties of thin films, which can improve the capability and reliability of industrial devices for magnetic recording and sensing.
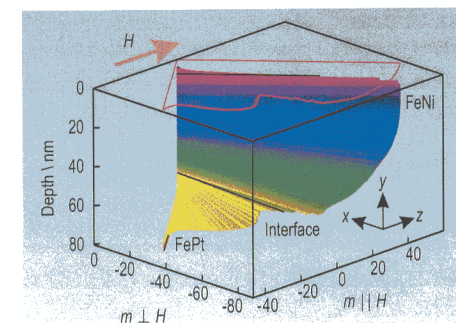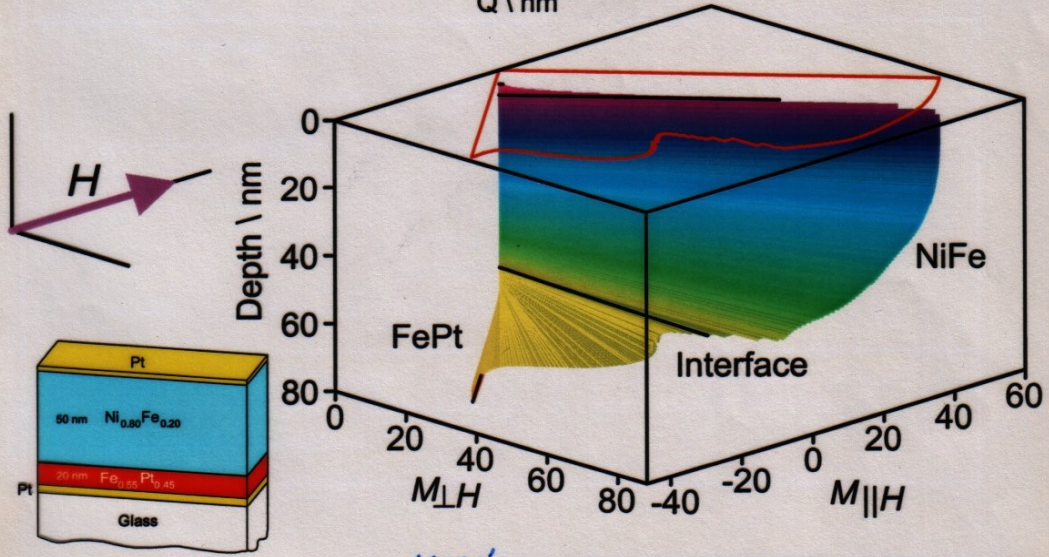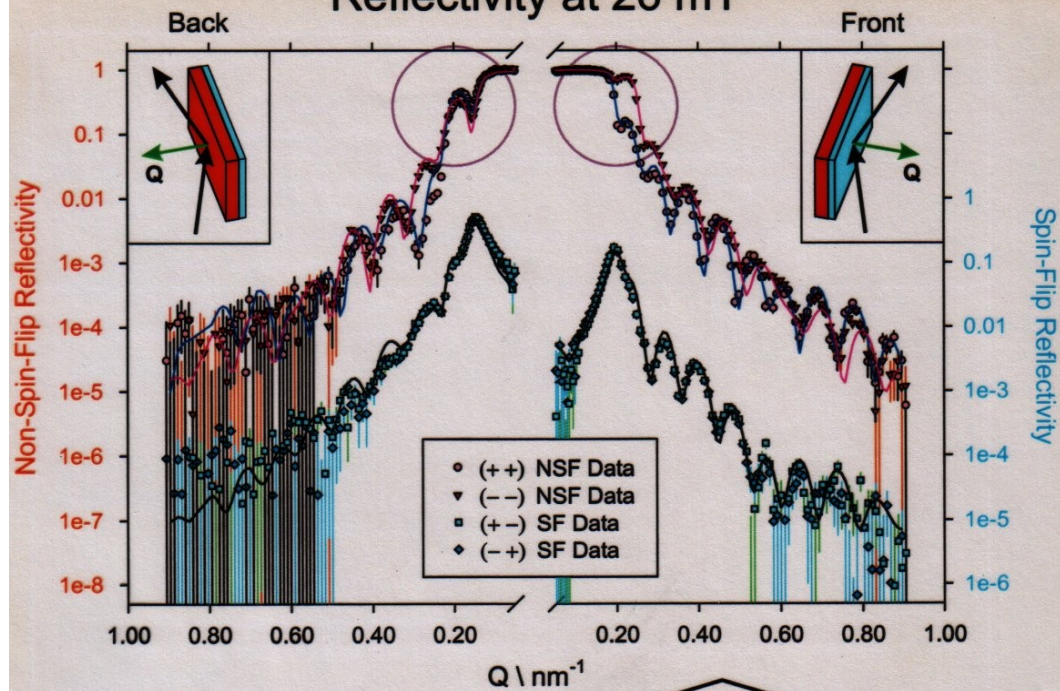


FIGURE 3. Fitted magnetization of the data presented in Fig. 2. The front of the sample is at a depth of 0 nm and the back is at a depth of 70 nm. The red curve is a projection of the magnetic structure into the plane of the front surface.

## References

[1] E. F. Kneller and R. Hawig, IEEE Trans. Magn. **27**, 3588 (1991).

[2] O. Hellwig, J. B. Kortright, K. Takano, and E. E. Fullerton, Phys. Rev. **B62**, 11694 (2000).

[3] K. V. O'Donovan, *et al.*, in preparation.

[4] K. V. O'Donovan, *et al.*, submitted to Applied Physics A.

# Reflectivity at 26 mT



**Back**

**Front**

Non-Spin-Flip Reflectivity

Spin-Flip Reflectivity

○ (+ +) NSF Data
▼ (− −) NSF Data
□ (+ −) SF Data
◆ (− +) SF Data

$Q \setminus nm^{-1}$

Depth \ nm

NiFe

FePt

Interface

$M \perp H$

$M \| H$

$H$

Pt
50 nm $Ni_{0.80}Fe_{0.20}$
Pt
20 nm $Fe_{0.55}Pt_{0.45}$
Glass

Deposited using magnetron sputtering
FePt codeposited from elemental targets
NiFe deposited from alloy target

K.V. O'DONOVAN, J.A. BORCHERS, C.F. MAJKRZAK, O. HELLWIG, E.E. FULLERTON

# *Magnetic Multilayers and Thin Films*
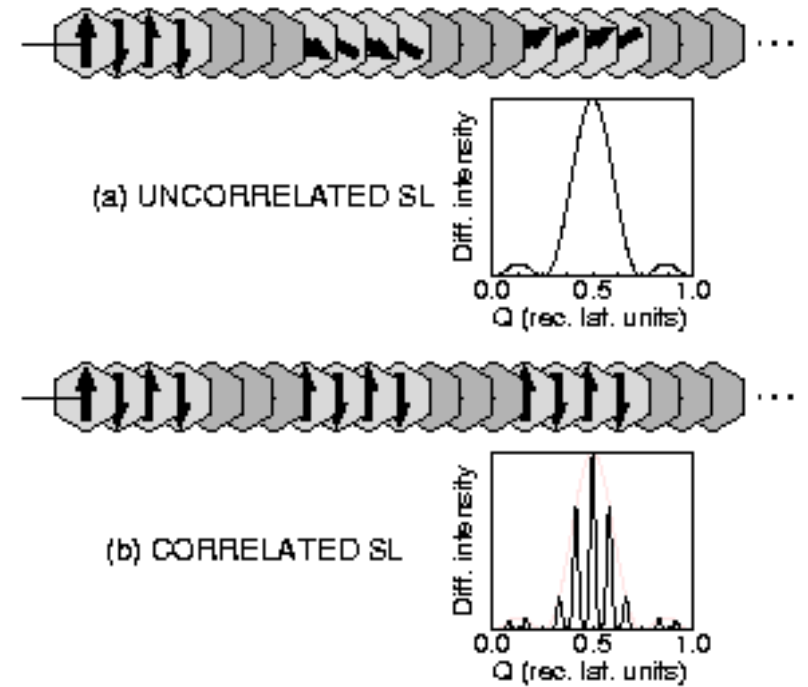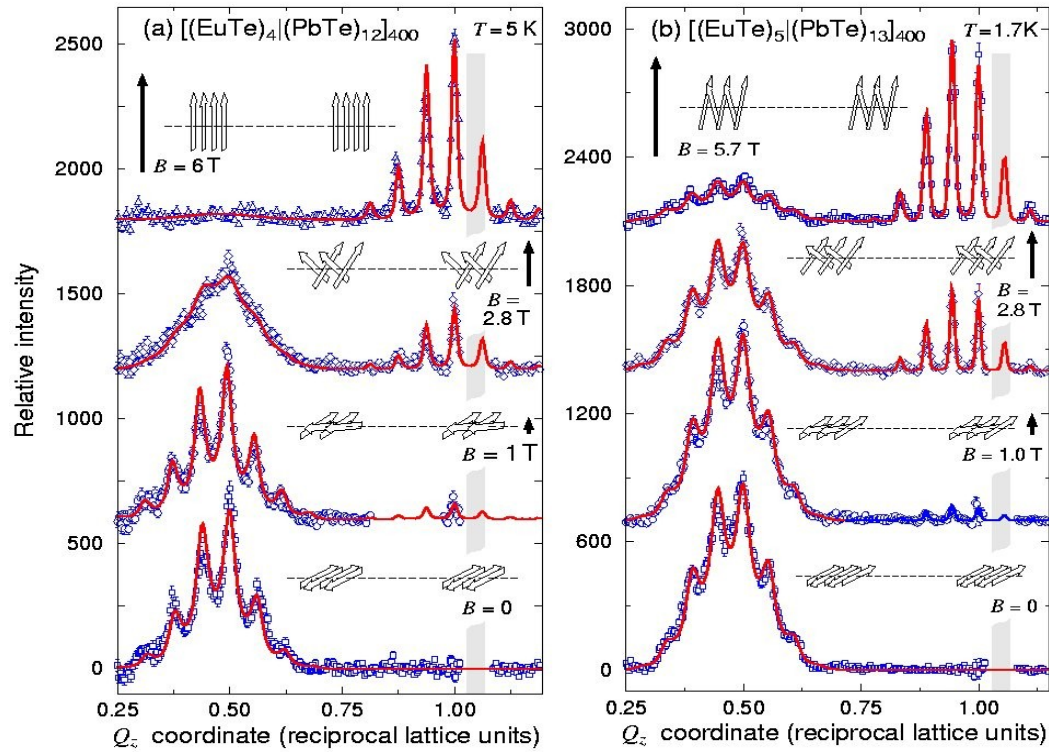


Polarized neutron reflection data on magnetic semiconductor superlattices by Henryk Kepa et al..
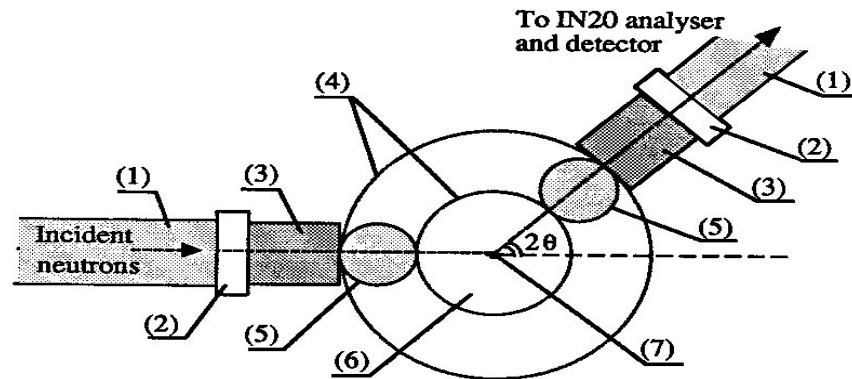
Fig. 3.2 Schematic horizontal cross-section of CRYOPAD showing: (1) axial guide field; (2) non-magnetic rotation unit; (3) nutation guide field (4) concentric test-tube shaped Meissner shields; (5) vertical super-conducting solenoids producing a precession field of up to 100 Oe; (6) zero field sample chamber containing a variable temperature insert which allows sample temperatures in the range 1.5 K to 300 K; (7) Sample position. Note that the contents of the cryostat tail are enlarged in the diagram for clarity - actual sizes are: inner Meissner screen diameter = 40 mm, precession solenoid diameter 13 mm, nutation guide diameter approximately 100 mm.
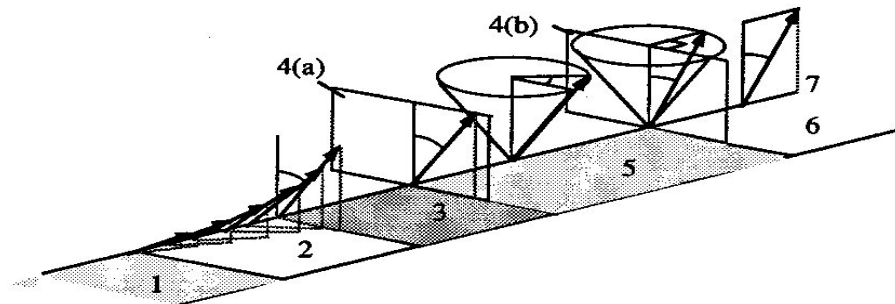


Fig. 3.4 Diagram showing what happens to the polarization of the incident neutrons during their passage through the different field regions of the instrument towards the sample position. In region (1), incident neutrons are polarized axially. In region (2), fields of (1) and (3) overlap, polarization rotates adiabatically to the direction of nutation field. As neutrons pass through the Meissner shield (4) the polarization is unchanged, then, in region (5), the polarization precesses around the vertical field axis. On reaching the second Meissner screen, neutron polarization has precessed by a total angle $\phi$, and once in zero-field (6), polarization is preserved up to sample position (7). Thus by choosing the angle of the nutation guide field and the current through the precession field, one can have any required direction of incident polarization at the sample position.

Zero-field neutron polarimetry ( figure from thesis of Valerie Nunez)

P.J.Brown, V.Nunez, F.Tasset, J.B.Forsyth and P.Radhakrishna
J.Phys.:Condens.Matter **2** (1990) 9409
**Determination of the magnetic structure of Mn$_3$S n using generalized neutron polarization analysis**

V.Nunez, P.J.Brown, J.B.Forsyth and F.Tasset
Physica B **174** (1991) 60
**Zero-field neutron polarimetry**

P.J.Brown, T.Chattopadhyay, J.B.Forsyth, V.Nunez and F.Tasset
J.Phys.:Condens. Matter **3** (1991)
**Antiferromagnetism in CuO studied by neutron polarimetry**

V.Nunez, P.J.Brown, T.Chattopadhyay, J.B.Forsyth and F.Tasset
Physica B - in print
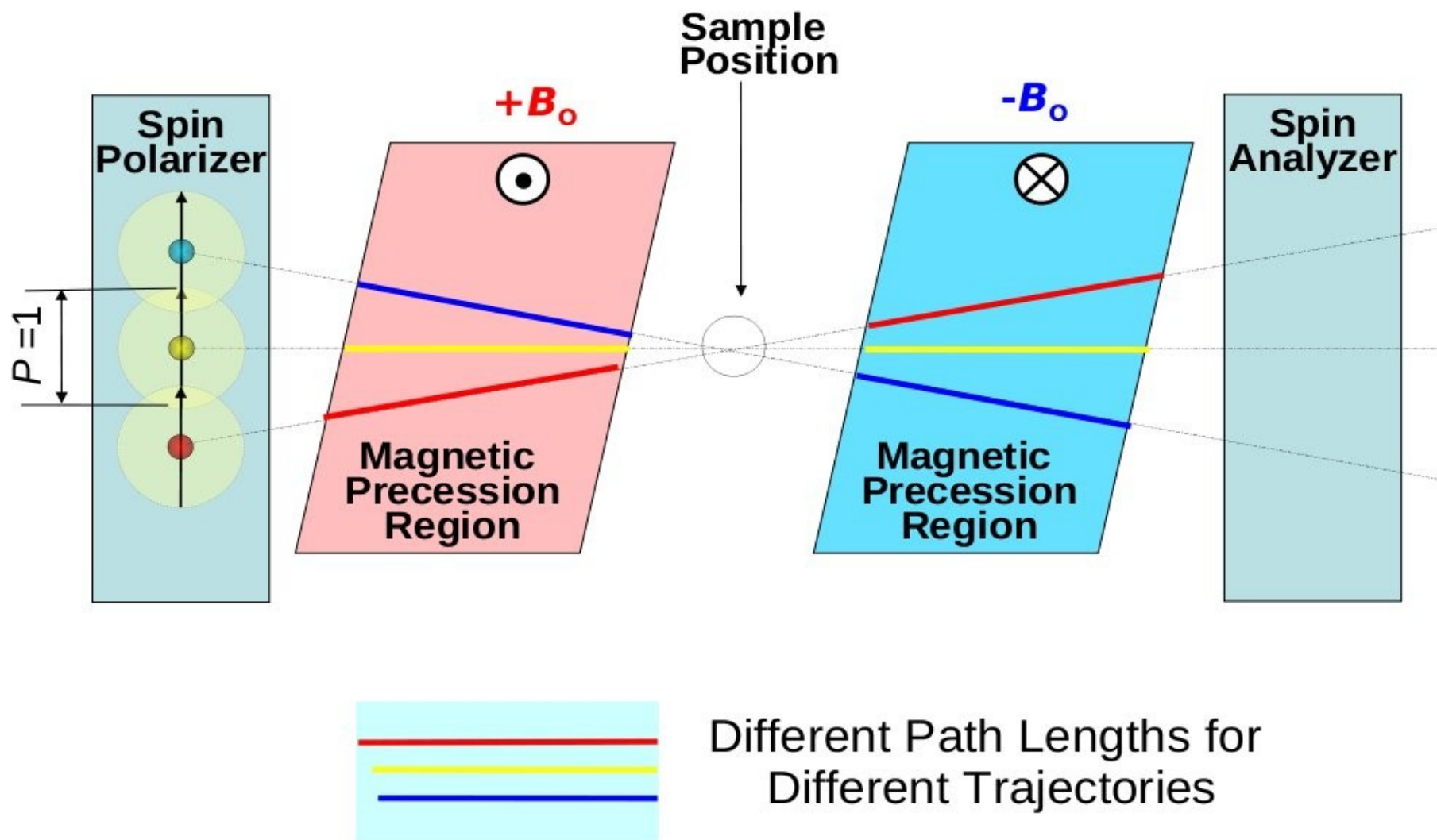**Magnetic structure determination using zero-field neutron polarimetry**

V.Nunez, R.Trump, P.J.Brown, T.Chattopadhyay, M.Loewenhaupt and F.Tasset
J.Phys.:Condens. Matter - submitted
**Antiferromagnetism of the Kondo lattice compound CeCu$_2$ studied by neutron polarimetry**
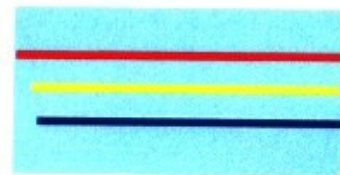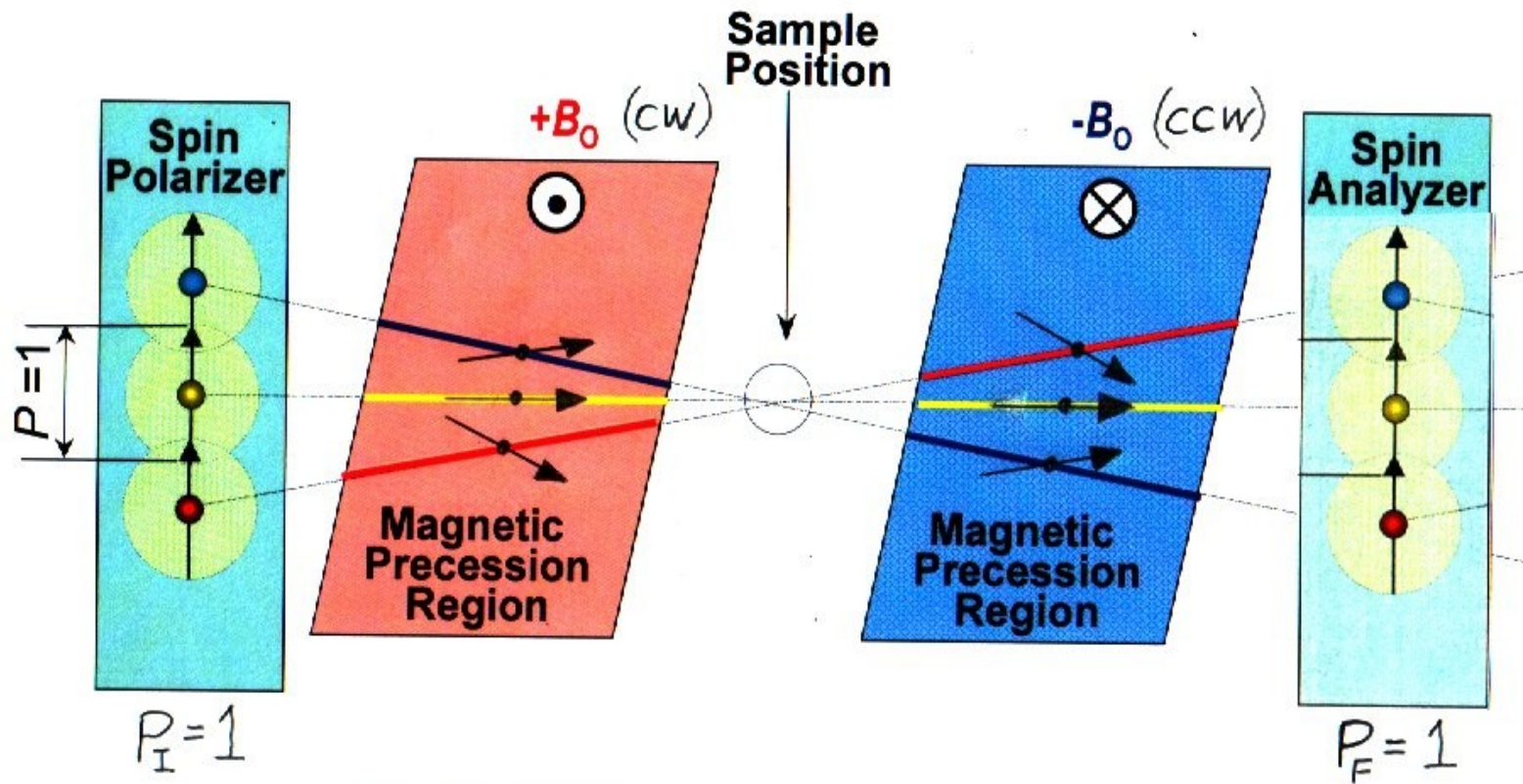
P.J.Brown, V.Nunez, F.Tasset and J.B.Forsyth
Acta Cryst. - submitted
**Extinction in mixed magnetic and nuclear reflections. A study of the magnetic structure of TbAlO$_3$ using zero-field neutron polarimetry and integrated intensity measurements**

## Part 3: Application of Polarized Neutrons to Measurements of Very Small Energy and Momentum Transfers with Condensed  Matter Systems
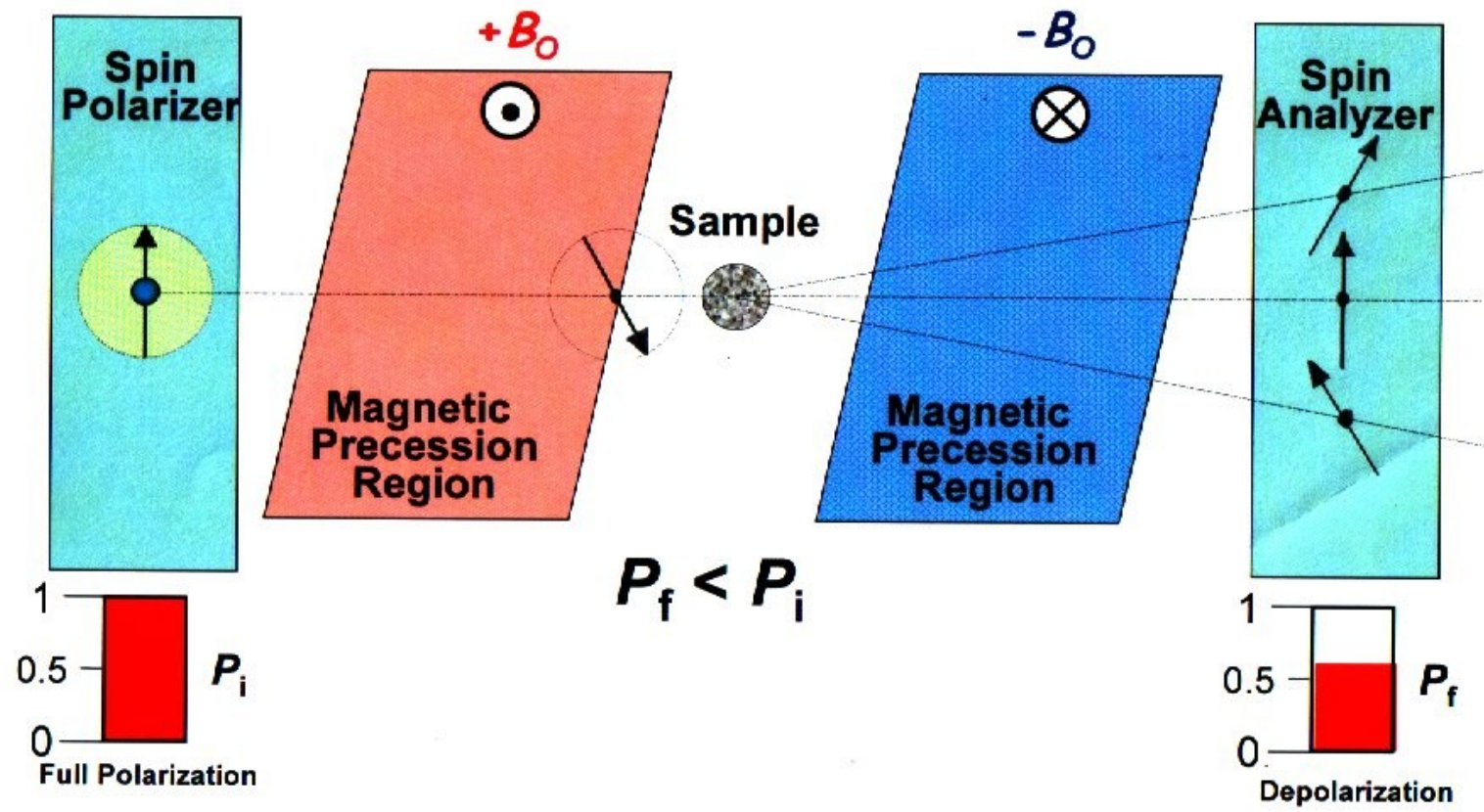
<> the precession of the neutron spin in a magnetic field can be used as an accurate measure of length from which changes in angle (momentum or wavevector direction) or neutron speed (energy or wavevector magnitude) can be determined

Neutron spin echo labelling of angle: after work of Felcher, te Velthuis, Rekveldt, Pynn, Major and others.  (Thanks to Suzanne te Velthuis for this and next figure!)



Sample Position

$+B_o$

$-B_o$

Spin Polarizer

Spin Analyzer

$P = 1$

Magnetic Precession Region

Magnetic Precession Region

Different Path Lengths for Different Trajectories

Sample Position

Spin Polarizer

$+B_0$ (cw)

$-B_0$ (ccw)

Spin Analyzer

$P = 1$

Magnetic Precession Region

Magnetic Precession Region

$P_I = 1$

$P_F = 1$

Different Path Lengths for Different Trajectories

Spin Polarizer

$+B_O$ ⊙

Sample

$-B_O$ ⊗

Spin Analyzer

Magnetic Precession Region

Magnetic Precession Region

$P_f < P_i$

$P_i$

Full Polarization

$P_f$

Depolarization

# NSE LABELLING OF ANGLE :
## PRECESSION FIELD GEOMETRY



SAMPLE

PRECESSION FIELD REGION

$$\phi = \alpha_F - \alpha_I$$

DEFLECTION OR SCATTERING ANGLE
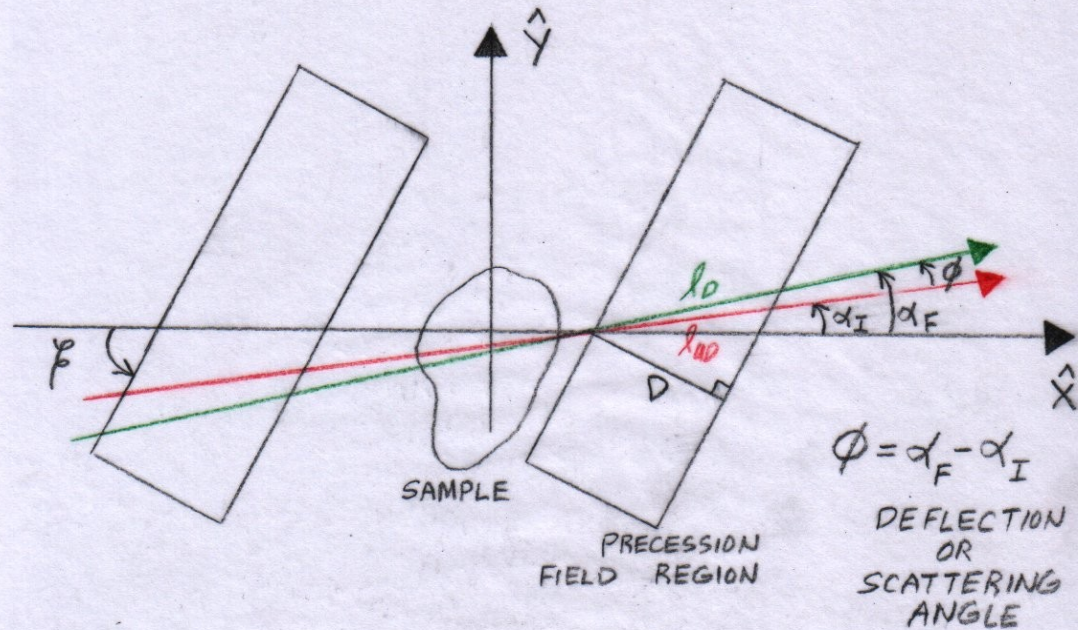
$$\ell_D \sin(\xi - \alpha_F) = D = \ell_{UD} \sin(\xi - \alpha_I)$$

PATH LENGTH DIFFERENCE $\quad \Delta \ell = \ell_D - \ell_{UD}$

$$\Delta \ell = D \left[ \frac{1}{\sin(\xi - \alpha_F)} - \frac{1}{\sin(\xi - \alpha_I)} \right]$$

AT SUFFICIENTLY SMALL ANGLES

$$\Delta \ell \simeq D \left[ \frac{(\alpha_F - \alpha_I)}{(\xi^2 - \alpha_F \xi - \alpha_I \xi + \alpha_F \alpha_I)} \right]$$

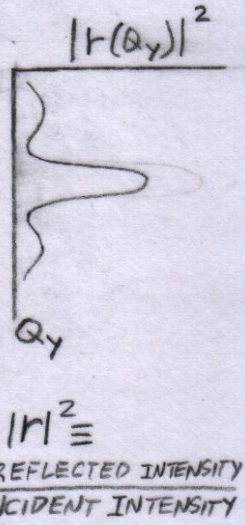# DIFFRACTION FROM GRATING STRUCTURE ALONG Y-DIRECTION (IN PLANE)

N INCIDENT BEAMS

$\hat{Y}_s$

PSD

$\alpha_F$

$\phi$

$\alpha_{Ij}$

$\alpha_{Ij}$

$\hat{Z}_s$

$\hat{X}_s$

$\phi = \alpha_F - \alpha_I$

SCATTERING ANGLE
OR
DEFLECTION ANGLE

$|r(Q_y)|^2$

$Q_y$
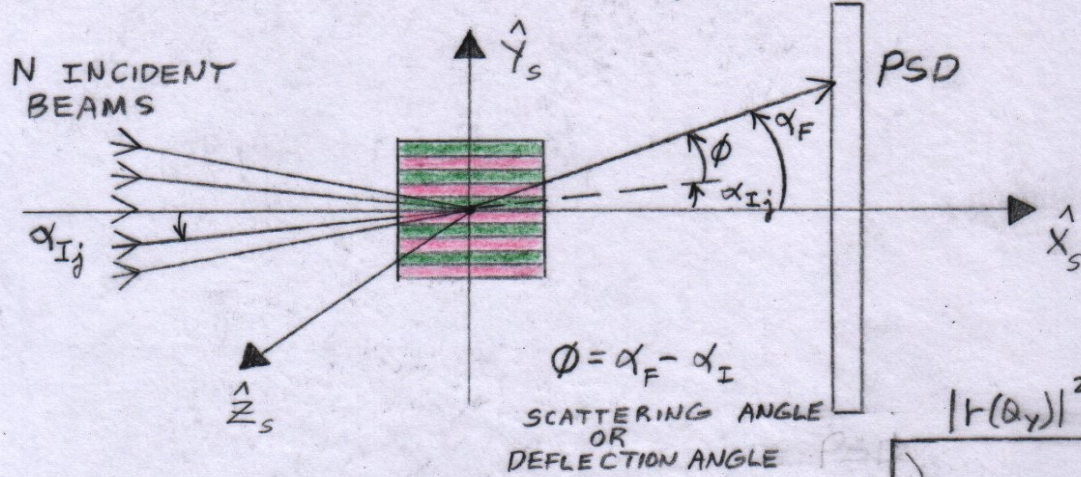
SOLVE SET OF SIMULTANEOUS EQUATIONS FOR $|r|^2$

$$S(\delta_i) = \sum_{j=1}^{N} I_0 \underbrace{M(\delta_i, \alpha_{Ij}, \alpha_F)}_{\text{MODULATION FUNCTION}} |r(\alpha_F, \alpha_{Ij})|^2$$

$S_1$
$S_2$
$\vdots$
$S_N$

($\delta_i$ = MODULATION PARAMETER)

$|r|^2 \equiv \dfrac{\text{REFLECTED INTENSITY}}{\text{INCIDENT INTENSITY}}$

e.g., $\quad M = \dfrac{I_{\pm}}{I_0} = \left[\dfrac{1 \pm \cos\beta}{2}\right]$

OR

$M = P_x = \dfrac{I_+ - I_-}{I_+ + I_-} = \cos\beta$

WHERE $\quad \beta = \text{CONSTANT } B \, \Delta l$

AND $\Delta l = \left[\dfrac{D(\alpha_F - \alpha_I)}{(\zeta^2 - \alpha_F \zeta - \alpha_I \zeta + \alpha_F \alpha_I)}\right]$

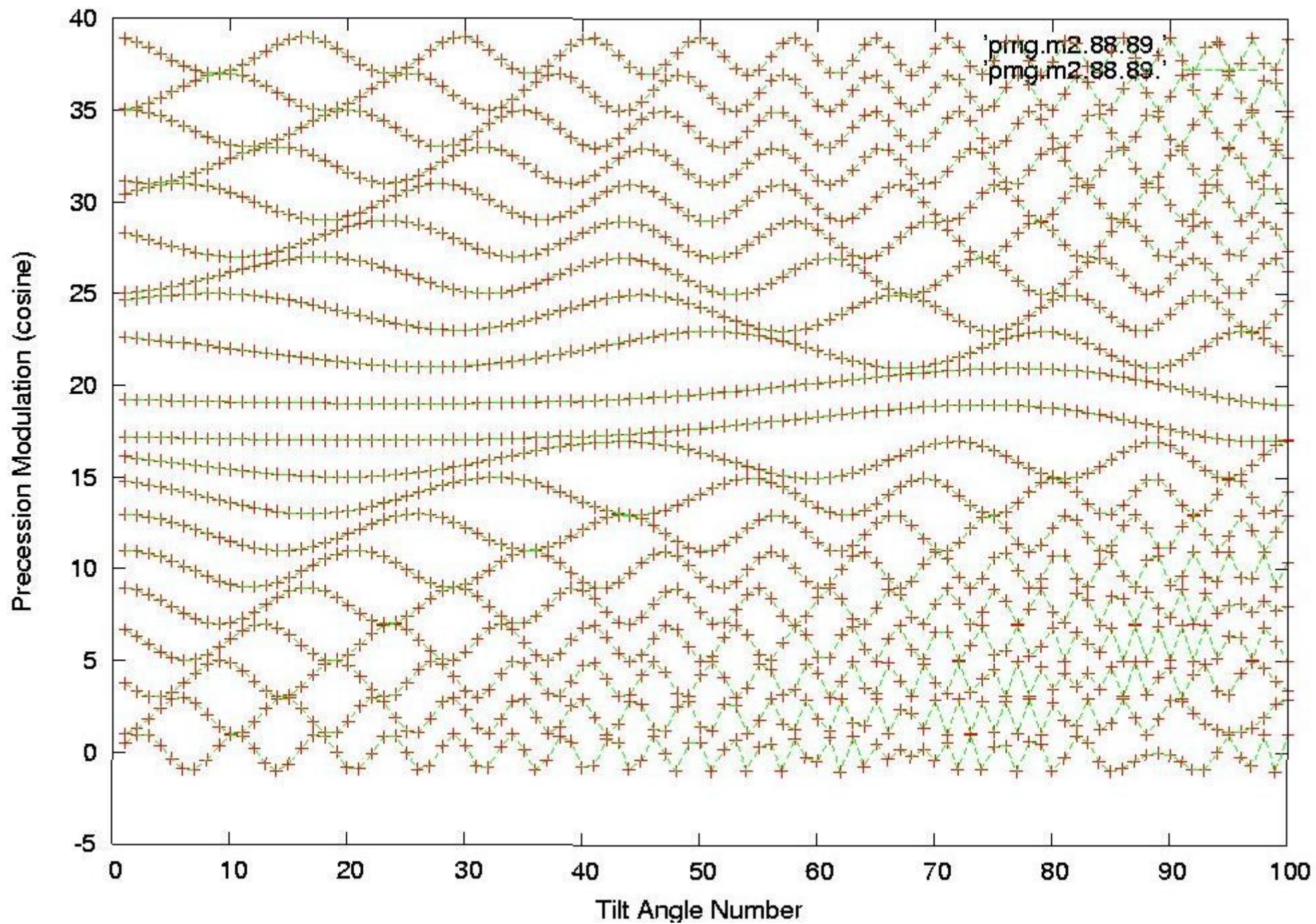$\zeta$ = "TILT" ANGLE OF RECTANGULAR PRECESSION FIELD REGION

$$Q_y \simeq k(\alpha_F - \alpha_I) \equiv k\phi$$
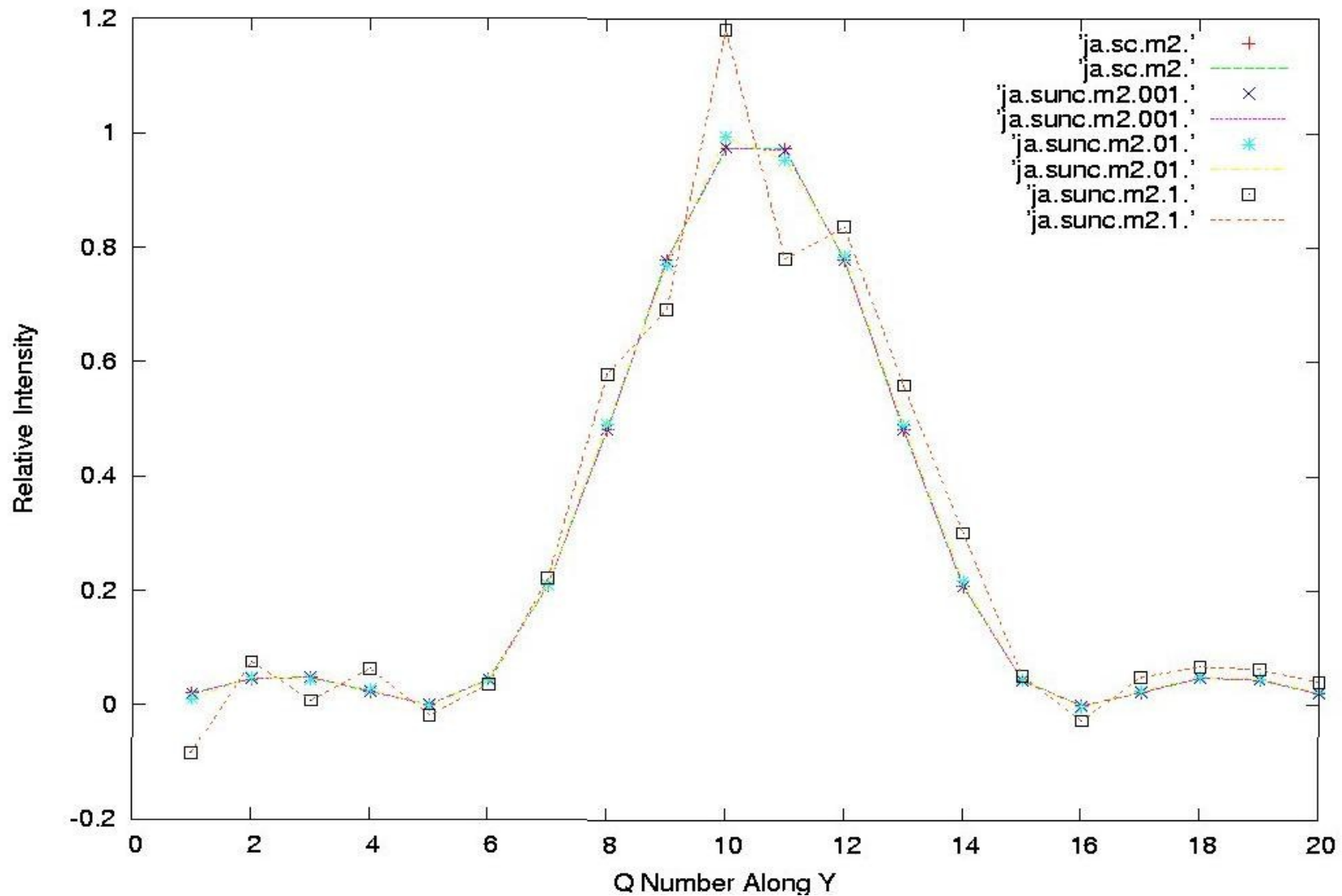
$$|r_{BA}(Q_y)|^2 \propto \left| \int \rho(y) e^{iQ_y Y} dy \right|^2$$

$$P_x(\delta^{SE}) = \int |r(\phi)|^2 \cos(k\phi\delta^{SE}) d\phi$$

WHERE $\quad \delta^{SE} = \left[ \left( \dfrac{m_m \gamma_m \lambda^2}{2\pi h} \right) \left( \dfrac{B\,D}{\sin\frac{\varepsilon}{2}} \dfrac{\cos\frac{\varepsilon}{2}}{\sin\frac{\varepsilon}{2}} \right) \right]$

$\underbrace{\phantom{\delta^{SE}}}$
SPIN ECHO "LENGTH"

$\underbrace{\phantom{\text{CONSTANT part}}}$
CONSTANT

PRECESSION FIELD TILT ANGLE

Comparison of inverted grating diffraction pattern to model where modulation of the beam was performed according to the spin-echo labeling method (blue asterisk symbols correspond to model and squares to calculated inversion).

# Compact magnetic films replace precession coils.



**Spin Echo Spectrometer**
on NG5 at the NCNR

**Spin Tagging Demonstration[1]**
on EVA at the ILL, France
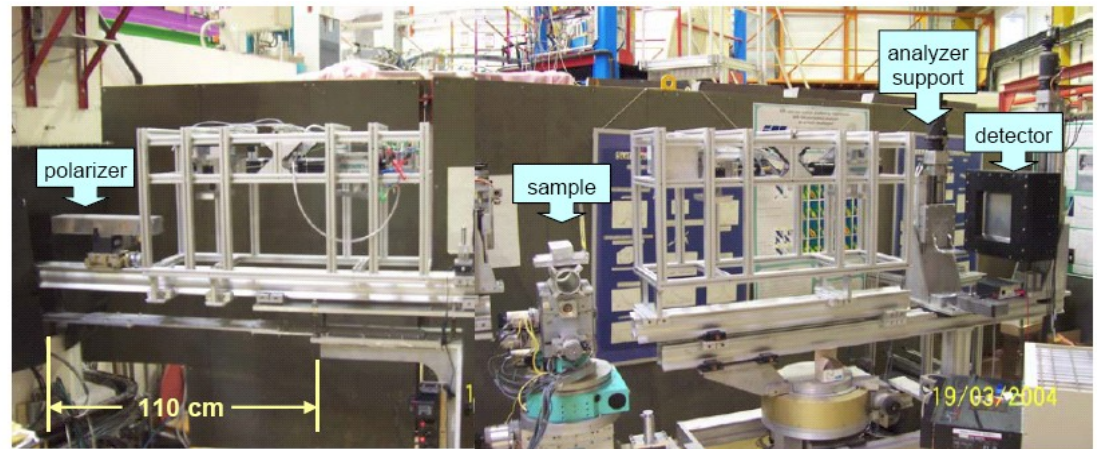


[1]J. Major, H. Dosch, G.P. Felcher, *et al*., Physica B (2003).
Also, M. Th. Rekveldt, *et al.,* Rev. Sci. Instr. (2005).
And  R. Pynn, M.R. Fitzsimmons, *et al*., Rev. Sci. Instr.  (2005).

"Polarized Neutron Reflectometry", C.F.Majkrzak, K.V.O'Donovan, and N.F.Berk, Chapter 9 in *Neutron Scattering from Magnetic Materials*, Edited by T.Chatterji, (Elsevier, Amsterdam, 2006) p.397-471.

*Polarized Neutrons*, W. Gavin Williams, (Clarendon Press, Oxford, 1988)